CHAPTER EIGHT

Ignimbrites and ignimbrite-forming eruptions

uced during
pyroclastic
sits resulting

Initial statement

Ignimbrites are the most voluminous of volcanic products. Some are the largest single eruptive units known, covering thousands of square kilometres and having volumes of more than 1000 km^3. Although man has never witnessed an eruption giving rise to such large volume units, they must be the most cataclysmic of all geological phenomena. Even small-volume, historic ignimbrite-forming eruptions are awesome: e.g. the 1470 BC eruption of Santorini, which has been linked with the rapid decline of the Bronze Age Minoan civilisation centre on Crete; the AD 79 eruption of Vesuvius, in which the towns of Pompeii and Herculaneum were destroyed; the eruption of Krakatau in 1883 which set in motion tsunamis killing more than 30 000 people on neighbouring islands; Tambora, which in 1815 caused the deaths of more than 90 000 people either directly, or as a result of tsunamis and an ensuing famine; Mt St Helens in 1980; and El Chichón in Mexico in 1982, after which 2000 people were missing.

This chapter examines in detail the geology of ignimbrites: definition, occurrence, volume, types of vent from which erupted, eruption sequence, a depositional facies model for ignimbrite-forming eruptions and welding. We also highlight the AD 186 Taupo eruption, because recent studies of its deposits have greatly affected current thinking on ignimbrite-forming events. Transportation and depositional mechanisms are discussed in the previous chapter.

8.1 Enigma of ignimbrites

Ignimbrites pose many problems but, as recently stated by G. P. L. Walker, unravelling their origin has been 'one of the outstanding success stories of modern volcanology'. They vary widely in lithology, and few products of volcanism have been misinterpreted for so long. They vary from incoherent ash deposits texturally similar to mud flows, to hard, densely welded tuffs which may be difficult to distinguish from lava flows. Indeed, welded ignimbrites were generally regarded as lava flows until the mid-1930s, and even later. They vary from rock composed almost entirely of sub-millimetre particles to that in which the largest clasts may be over a metre in diameter. Many ignimbrites are completely non-welded, but the importance of these was probably not recognised until the late-1960s and early-1970s.

It will be apparent to the reader who has researched the volcanological literature that the term '*ignimbrite*' has been used in many different ways. Marshall (1935) first introduced the term into the geological literature. Confusion, partly attributable to the imprecision of Marshall's definitions, has arisen and still exists because 'ignimbrite' is sometimes used in a lithological sense to mean welded tuff, and sometimes in a genetic sense to mean the rock or deposit formed from pyroclastic flows. Very often the term is used in both senses, or it is used in ways that are never clearly defined. However, it is illogical to use it as a lithological term solely for welded rocks, since ignimbrites generally also have non-welded zones. The occurrence of welding has occasionally been cited as sufficient evidence of a pyroclastic flow origin. However, even many large ignimbrites are entirely non-welded, e.g. the Los Chocoyos ash-flow tuff in Guatemala (Table 8.1). Also, welded *air-fall* tuffs are believed to be a common volcanic rock (Ch. 6). Welding cannot therefore be considered to be a fundamental characteristic of ignimbrites.

Following Sparks *et al.* (1973) 'ignimbrite' is defined here as: the rock or deposit formed from pumiceous pyroclastic flows irrespective of the degree of welding or volume. 'Pumice-flow deposit' is an equivalent term (Ch. 5).

Table 8.1 Bulk volume estimates of some ignimbrites*

Deposit	Volume (km³)
USA	
Timber Mountain Tuff	
Rainier Mesa Member	1200
Ammonia Tanks Member	900
Paintbrush Tuff	
Topopah Spring Member	250
Tiva Canyon Member	1000
Nelson Mountain Tuff	500
Carpenter Ridge Tuff	500
Fish Canyon Tuff	3000
Sapinero Mesa Tuff	1000
Upper Bandelier Tuff	200
Bishop Tuff	500
Peach Springs Tuff	90
John Day pyroclastic flow deposit	75
Crater Lake pumice-flow deposit	25
Valley of Ten Thousand Smokes ignimbrite	12
Central and South America	
Rio Caliente ignimbrite	30
Acatlan ignimbrite	5
Los Chocoyas ash-flow tuff	200
Apoyo pyroclastic flow deposit	5
Puncipar ignimbrite	100
El Yeso ignimbrite	40
Cerro Galan ignimbrite	1000
Lesser Antilles	
Roseau ignimbrite†	30
Average Belfond pumice flow deposit on St Lucia	0.2
Iceland	
Skessa welded tuff	4
Rovdarfjordur tuff	2.5
Matarhnjkur welded tuff	1
Mediterranean	
average of six ignimbrites erupted from Vulsini volcano	6
Vesuvius AD 79	4
Campanian ignimbrite	100
Minoan ignimbrite†	30
Japan	
Ito pyroclastic flow deposit	110
Aso III pyroclastic flow deposit	175
Kutcharo welded tuff	90
Akan welded tuff	60
Hakone pyroclastic flow deposit	15
Hijori pyroclastic flow deposit	1.4
Kuttara welded tuff	10

Deposit	Volume (km³)
Mashu pyroclastic flow deposit	5
Numajiri welded tuff	1.2
Tazawara welded tuff	150
Tokachi welded tuff	60
Tokachidake 1926 pumice-flow deposit	0.02
Agatsuma pyroclastic flow deposit	0.1
Asama pumice-flow deposit I	2
Asama pumice-flow deposit II	1
Komagatake 1929 pyroclastic flow deposit	0.15
Nantai pumice-flow deposit	0.8
Shikotsu pyroclastic flow deposit	80
Towada pyroclastic flow deposit I	25
Towada pyroclastic flow deposit II	25
Indonesia	
Toba Tuff	2000
Bali ignimbrite	20
Tambora 1815	25
Krakatau 1883†	12
New Zealand	
Ongatiti ignimbrite	190
Whakamaru ignimbrite	150
Matahina ignimbrite	100
Taupo ignimbrite	30

* There are many problems with such a survey of the literature. First, data from which estimates have been made vary from detailed maps and volcanological studies to simply gross estimates. Secondly, a significant or major part of some ignimbrites is welded tuff, but the proportion of welded to non-welded material is generally not given; therefore, no allowance is made for compaction although this is an important factor when making size comparisons. Thirdly, published studies have tended to describe the larger, more spectacular ignimbrites. Note also that the volume lost into a co-ignimbrite ash fall deposit is not included in these estimates.

† Major part deposited in sea as subaqueous 'pyroclastic flow' deposits and ash turbidites (Ch. 9).

Based on the supposed dominance of ash-sized particles in pyroclastic flows, R. L. Smith (1960a, b) and Ross and Smith (1961) introduced the term 'ash-flow tuff', which is extensively used throughout the American literature. However, as the modal grainsize in many pumice-flow deposits is in the lapilli or bomb size range, such deposits would therefore not strictly come under the definition of ash-flow tuff. For this reason the 'English school' has tended to retain the term 'ignimbrite'. It is unlikely that either term will be dropped from the literature.

Also, '*nuée ardente*' has sometimes been used for 'ignimbrite', as well as for other types of pyroclastic flows (Chs 5 & 12). If used, 'nuée ardente' should be restricted to those small-volume block and ash flows produced by the collapse of an actively growing lava flow or dome, as originally described by La Croix from the 1902 eruption of Mt Pelée (La Croix 1904). Nowadays we tend to avoid the term, not only because it has become ambiguous, but also because there are other more-specific terms, and most of the 'glowing cloud' forms ash-cloud surge and ash fall deposits.

8.2 Occurrence, composition and size

Ignimbrites are common volcanic products, being found in all volcano-tectonic settings: oceanic islands (e.g. Iceland, Azores and Canary Islands), island arcs (Lesser Antilles), microcontinental arcs (New Zealand), continental margin arcs (Andes) and continental interiors (Western USA). Rhyolite, dacite and andesite are the most common compositions. Many of the most voluminous ignimbrites are rhyolites, some of which are compositionally zoned, indicating in some cases the tapping of large zoned magma chambers (R. L. Smith 1979). Ignimbrites can have alkaline compositions, e.g. in the Azores, Tenerife, Philippines and Italy (Ch. 13). Pantelleritic ignimbrites have been recorded from a number of areas, e.g. the East African Rift, Gran Canaria and the Western USA. Ignimbrites have been recognised in geological formations of all ages.

In size, ignimbrites range over at least five orders of magnitude of volume. The largest are restricted in their occurrence to continental margins and interiors, and large islands. They typically result from eruptions of silicic calc-alkaline magmas, and tend to form extensive sheets or shields (Ch. 13). The smallest are found in all settings and are a common product of stratovolcanoes, although not restricted to this type of centre (Ch. 13). These tend to form valley fill deposits, and their distribution may be localised and their stratigraphy very complex. Figures 8.1–8.7 illustrate the distributions of some selected ignimbrites. Note the differences in

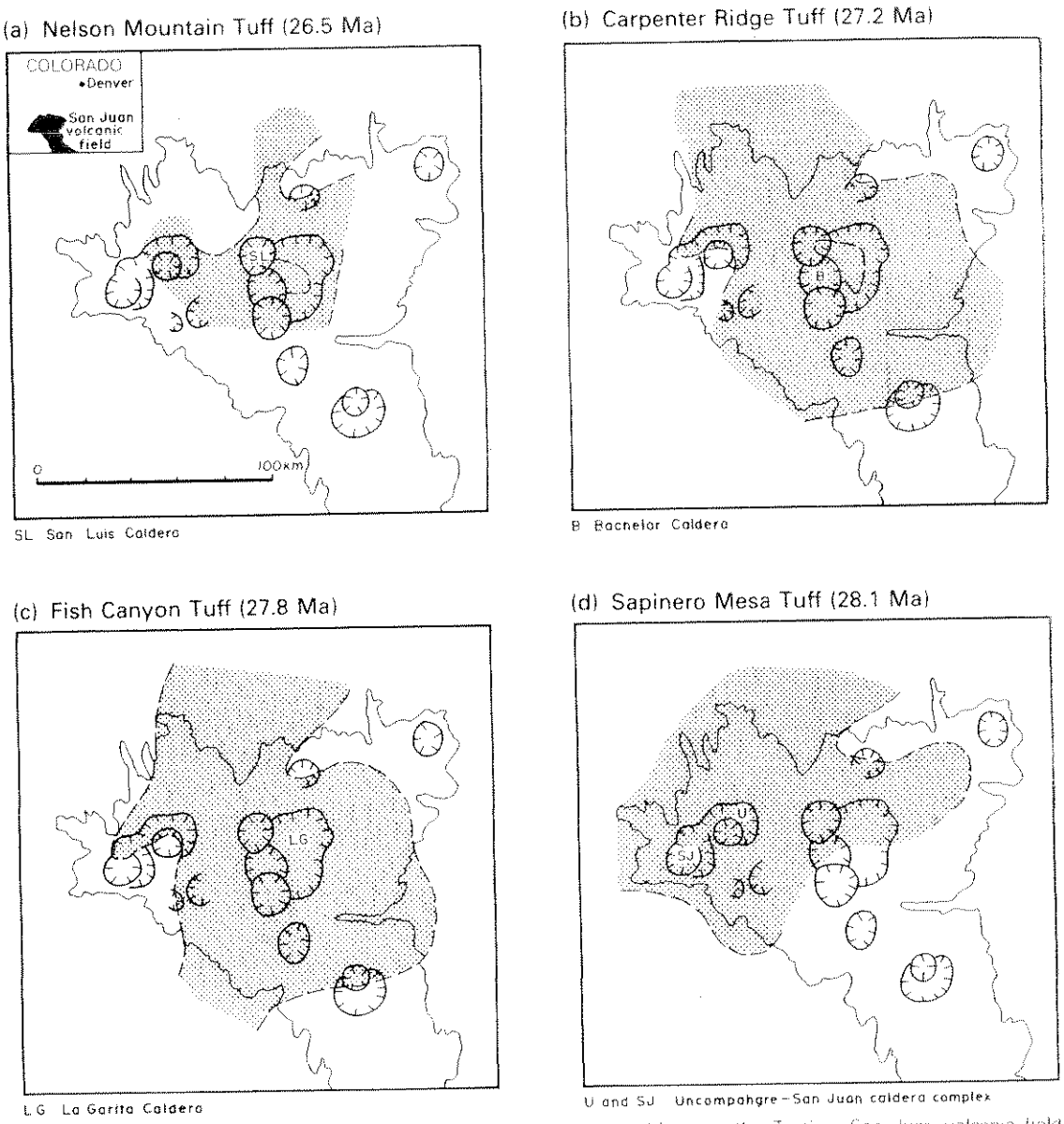

Figure 8.1 Examples of large ignimbrite sheets and associated calderas in the Tertiary San Juan volcanic field, Colorado. For the most part they are densely welded tuffs. Note that these maps only show schematic original distribution, not present outcrop pattern, which is very complex because of erosion. (After Steven & Lipman 1976.)

scales between maps; there is a 24-fold difference between maps showing examples from the San Juan volcanic field in Colorado and the Mt St Helens 1980 deposit.

Table 8.1 lists the estimated volumes of a number of ignimbrites. Most of the largest ignimbrites described are those associated with large calderas in the Western USA, and in many cases are, for the most part, densely welded tuff. The world's biggest is the Fish Canyon Tuff in the San Juan volcanic field (Fig. 8.1c) which is thought to have a minimum volume of 3000 km^3. An enormous

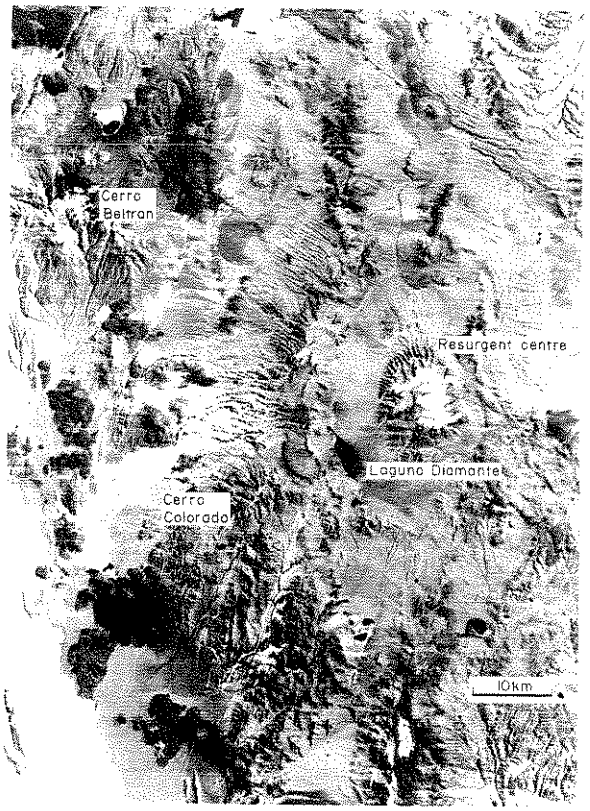

Figure 8.2 A LANDSAT image showing the giant Cerro Galan ignimbrite and caldera in northwestern Argentina. Extensive ignimbrite shield is seen as pale-toned, regularly dissected smooth expanses, best displayed on the northern flanks. The snow-capped resurgent dome (6100 m above sea level) is conspicuous in the middle of the caldera. Laguna Diamante is a relic of a much larger lake which may have filled the caldera before resurgence. Cerro Colorado and Cerro Beltran are pre-caldera andesitic stratovolcanoes. Dark areas west of Cerro Colorado are basaltic andesite scoria cones and lava flows broadly contemporaneous with the ignimbrite. (After P. W. Francis *et al.* 1983.)

part of these large deposits occurs as thick intracaldera ignimbrite, while smaller volumes are found as outflow sheets. Later updoming of the intracaldera pile may form a resurgent dome (Fig. 8.2, Ch. 13).

In Table 8.2, the maximum distance travelled from the source vent is given for a number of ignimbrites. The data demonstrate the ability of pumice flows to travel large distances, often over gently sloping ground and sometimes over topographic barriers (also see Figs 7.2, 17, 18 & 21).

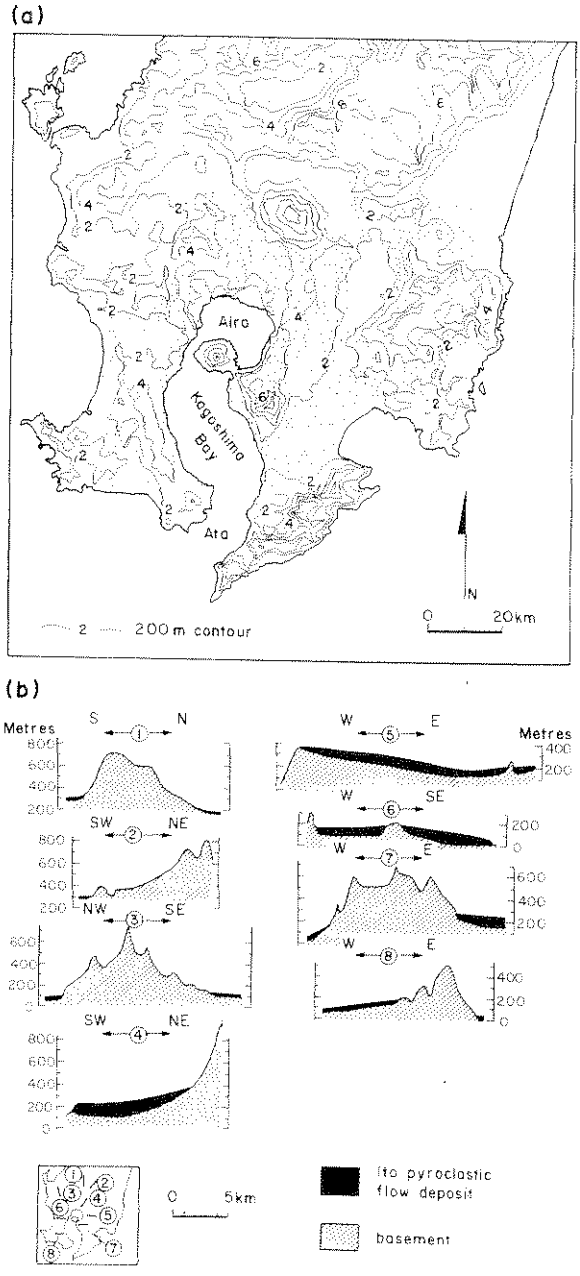

Figure 8.3 Ito pyroclastic flow deposit from Aira caldera, Japan, erupted about 22 000 years BP. Its eruption is thought to have produced the Aira caldera. (a) and (b) show the complex distribution pattern of the ignimbrite, and the topography that the (one) pumice flow was capable of climbing. cross section 4 shows a good example of depositional ramping (Section 8.8). The ignimbrite is largely non-welded. (After Yokoyama 1974.)

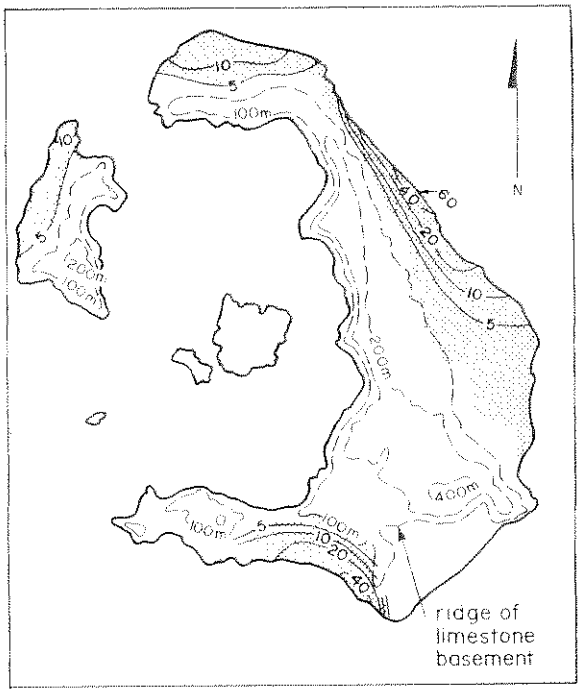

Figure 8.4 Isopach map of the Minoan ignimbrite, Santorini

Table 8.2 Maximum distances travelled from source by some ignimbrites*

Ignimbrite	Distance (km)
Timber Mountain Tuff	
Rainier Mesa Member	76
Paintbrush Tuff	
Topopah Springs Member	60
Nelson Mountain Tuff	50
Fish Canyon Tuff	100
Sapinero Mesa Tuff	110
Upper Bandelier Tuff	30
John Day pyroclastic flow deposit	75
Crater Lake pumice-flow deposit	58
Valley of Ten Thousand Smokes ignimbrite	22
Aniakchak ash-flow tuff	50
Fisher ash-flow tuff	30
Mt St Helens 1980	8
Rio Caliente ignimbrite	20
Acatlan ignimbrite	20
Puripicar ignimbrite	35
Cerro Galan ignimbrite	70
Ignimbrite A Vulsini volcano	17
Ignimbrite C Vulsini volcano	27
Ito pyroclastic flow deposit	80

Table 8.2 *continued*

Ignimbrite	Distance (km)
Aso III pyroclastic flow deposit	70
Hakone pyroclastic flow deposit	18
Ata ash-flow tuff	60
Shikotsu pyroclastic flow deposit	40
Bali ignimbrite	40
Whakamura ignimbrite	48
Morrinsville ignimbrite	225
Taupo ignimbrite	80

* Erosion probably makes many of these measurements underestimates

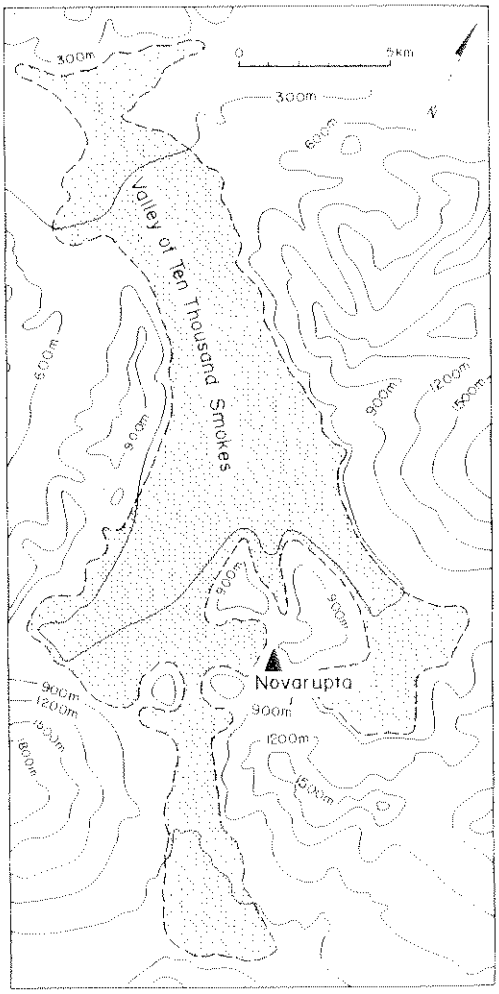

Figure 8.5 Valley of Ten Thousand Smokes ignimbrite (after C. N. Fenner 1920 and Curtis 1968)

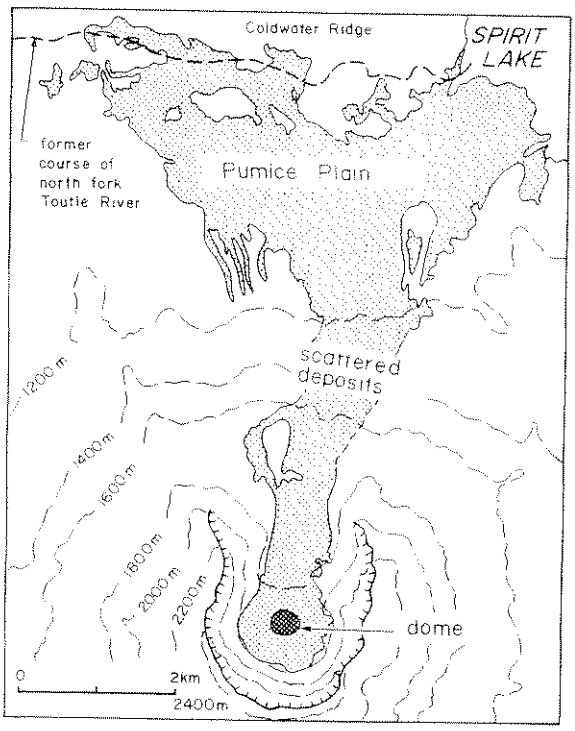

Figure 8.6 Distribution of Mt St Helens 1980 pumice-flow deposits. (After Rowley *et al.* 1981.)

8.3 Eruption sequence and column collapse

Most studies of the stratigraphic relations within ignimbrites and interpretive analysis of their eruptions have been made on small- to medium-volume (<1 a few hundred cubic kilometres) deposits. These often indicate a common sequence of activity (Sparks *et al.* 1973; Plate 8):

(a) plinian phase producing a pumice-fall deposit (Ch. 6),
(b) pyroclastic flow-phase producing ignimbrite and pyroclastic surges and
(c) effusive-phase producing lava (Ch. 4).

This sequence is thought to represent the tapping of deeper and less gas-rich levels of the magma chamber. A consequence is that a plinian eruption will be driven towards an ignimbrite-forming one as its column overloads and collapses to generate pyroclastic flows (Fig. 8.8). Theoretical modelling has shown that the change from plinian to ignimbrite-forming activity varies with vent radius, gas velocity and H_2O content (L. Wilson 1976, Sparks & L. Wilson 1976, L. Wilson *et al.* 1978, 1980; Ch. 6). Collapse occurs at a critical level of magma water content, given a constant vent radius and muzzle velocity. Widening or flaring of the vent during the eruption will also drive the column towards collapse conditions. The fountain height of the collapsing column as a function of gas content and vent radius is shown in Figure 8.9. Scenarios of three model ignimbrite-forming eruptions (Fig. 8.10) show the variations in column height and gas velocity that take place as the conduit is eroded and gas content decreases during the course of an eruption. In the first case (Fig. 8.10a), vent radius changes while exsolved water content remains constant at 3.45 wt%. The eruption column height grows steadily until sudden collapse occurs and a low ignimbrite-forming fountain is established. Eruption velocity in the vent slowly increases throughout the eruption. In the second case, vent radius increases and exsolved gas content decreases. Variation in height of the eruption column is similar to that found in the first case, though fountain height decreases after the collapse event. Eruption velocity decreases throughout the eruption, due to the falling gas content. In the third case, vent radius remains fixed and gas content decreases during the eruption. There is a much smaller variation in plinian column height than in the first two cases. Again, fountain height gradually decreases after the collapse event.

In Figure 8.11a, combinations of the controlling parameters are plotted and fields of convecting plinian and collapsing columns are shown. From a knowledge of the stratigraphy of a deposit, and by estimating values of the controlling parameters, it is now possible to track the progress and changes in energetics of an eruption to a first-order approximation. Three examples are shown in Figures 8.11b, c and d. Eruptions which terminate before column collapse conditions are reached will only produce plinian fall deposits (Fig. 8.11b; Ch. 6). S. N. Williams and Self (1983) suggested that the Santa Maria 1902 eruption resulted from release of volatile-rich magma at the top of a volatile stratified

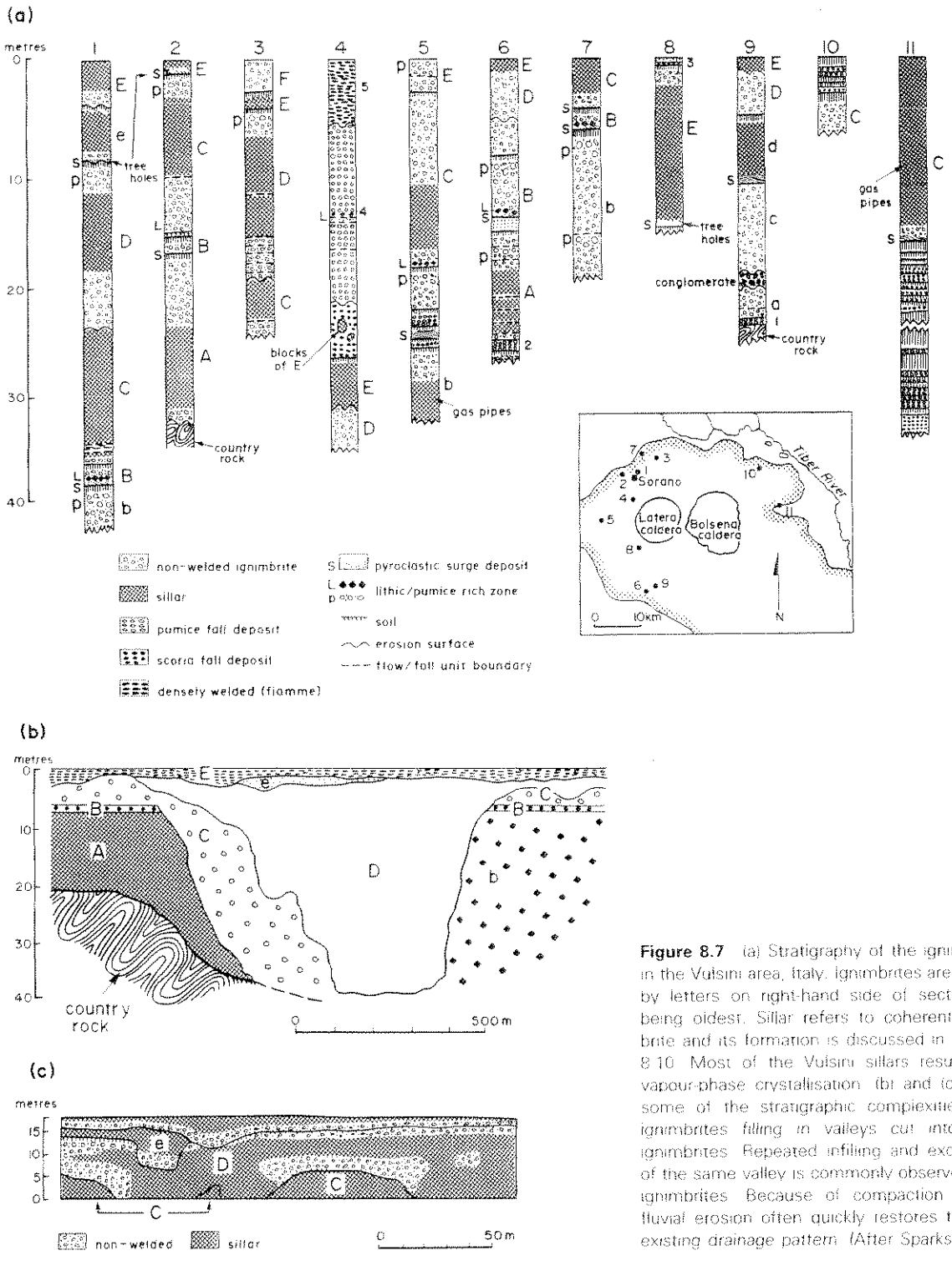

Figure 8.7 (a) Stratigraphy of the ignimbrites in the Vulsini area, Italy. Ignimbrites are named by letters on right-hand side of sections, A being oldest. Sillar refers to coherent ignimbrite and its formation is discussed in Section 8.10. Most of the Vulsini sillars result from vapour-phase crystallisation. (b) and (c) show some of the stratigraphic complexities with ignimbrites *filling in* valleys *cut into older* ignimbrites. Repeated infilling and excavation of the same valley is commonly observed with ignimbrites. Because of compaction effects fluvial erosion often quickly restores the pre-existing drainage pattern. (After Sparks 1976.)

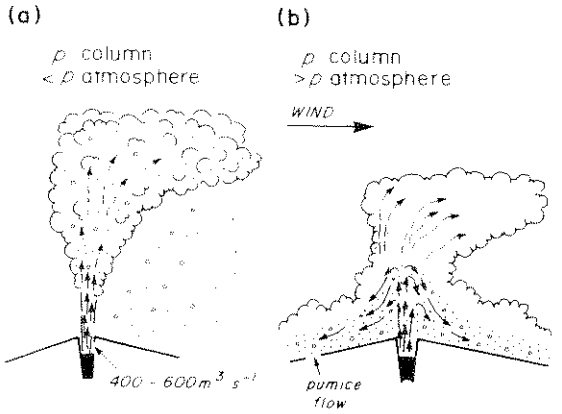

Figure 8.8 Models of eruption columns formed during ignimbrite volcanism: (a) plinian and (b) ignimbrite-forming.

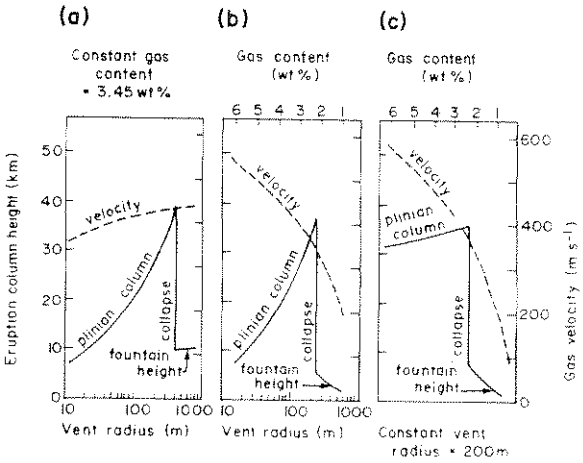

Figure 8.10 Scenarios of three model ignimbrite-forming eruptions (see text). (After L. Wilson *et al.* 1980.)

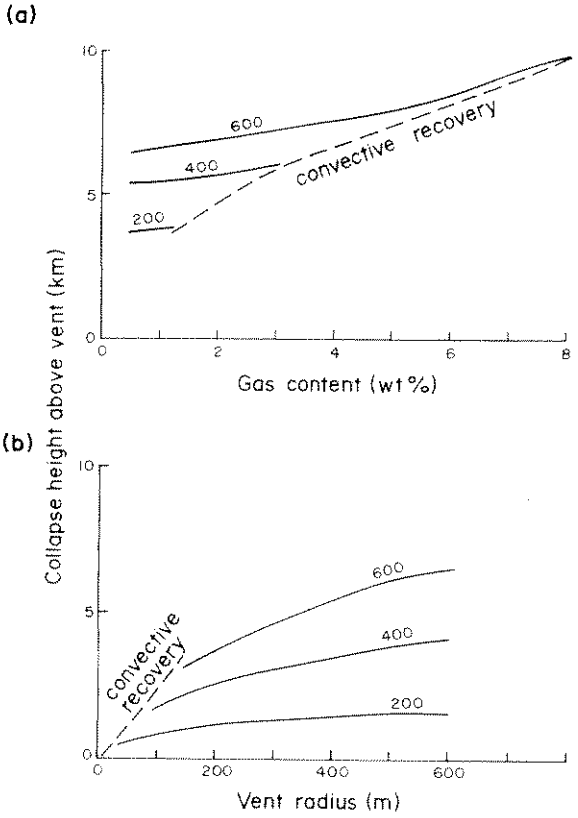

Figure 8.9 Fountain height of collapsing ignimbrite-forming eruption columns. (a) Plotted as a function of gas content for three vent radii for a constant gas velocity of 600 m s^{-1}. (b) Plotted as a function of vent radius for three gas velocities. The collapse height is only slightly affected by water content, but the computations shown here refer to a value of 1%. (After Sparks *et al.* 1978.)

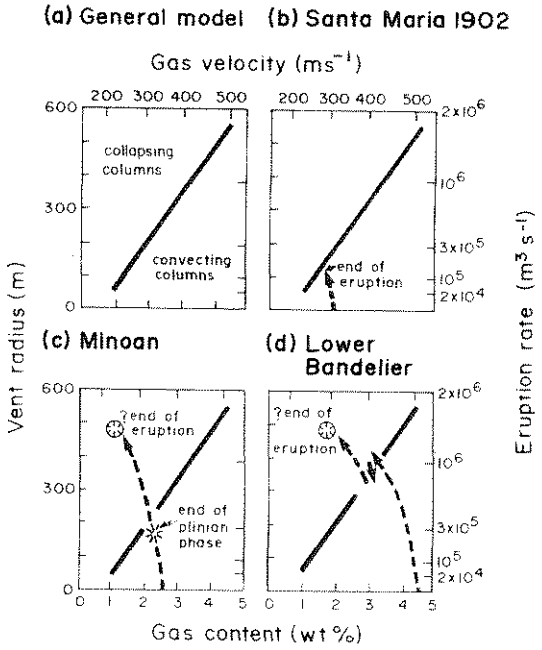

Figure 8.11 (a) General model showing plot of vent radius, gas content, eruption rate and gas velocity, relating these parameters to convecting plinian and collapsing ignimbrite-forming eruption columns (after L. Wilson *et al.* 1980). (b)–(d) Changing conditions during three eruptions (after S. N. Williams & Self 1983, L. Wilson 1980a and Self & Wright *unpub. data*).

magma chamber. As the eruption proceeded, less volatile-rich magma was encountered and structural instabilities caused collapse of the conduit walls, abruptly shutting off the magma supply. The remaining magma was unable to generate sufficient volatile pressure to clear the conduit, and the plinian phase ended; it was 20 years later when volatile-poor magma reached the surface as a lava. The Minoan plinian column was maintained until collapse conditions developed (Fig. 8.11c), although a phase of phreatomagmatic activity between the plinian and pyroclastic flow-forming phases may have complicated the transition between the two. As the Lower Bandelier plinian column neared the point of collapse (Fig. 8.11d), slight fluctuations in gas velocity and mass discharge rate caused instabilities in the column and small-volume intraplinian flow units to form (Fig. 6.13b). Catastrophic column collapse ensued. Instabilities in eruption columns nearing collapse conditions would account for the stratification found at the tops of many plinian deposits (Ch. 6).

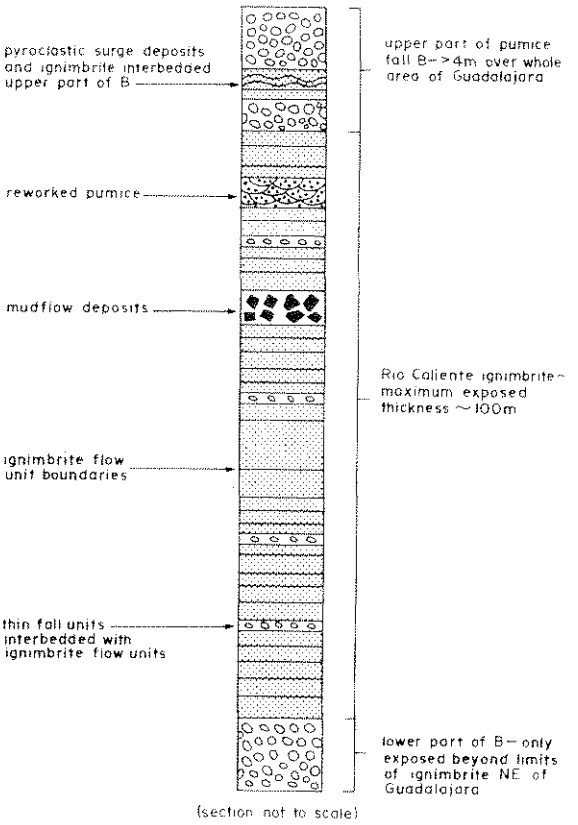

Figure 8.12 Generalised stratigraphic section showing the complex eruption sequence of the Rio Caliente ignimbrite, Mexico, and co-eruptive plinian falls (designated La Primavera B, Ch. 6). (After J. V. Wright 1981.)

Some deposits show much more complex eruption sequences than indicated above, and ignimbrite flow units are interstratified with plinian fall units, e.g. the Rio Caliente ignimbrite Mexico (Fig. 8.12) and the Roseau Tuff, Dominica (Ch. 9). The Rio Caliente can also be described as an **intraplinian** ignimbrite because it is sandwiched between two co-eruptive plinian fall deposits. Mechanisms to produce such complex sequences and changes in style of activity include a large increase in gas content, increasing proportions of low molecular weight volatiles, and sudden closure of the vent by faulting and its relocation. Choking of the vent by wall collapse may also produce alternations from ignimbrite-forming to plinian activity, especially if column conditions are close to the boundary between convection and collapse (Ch. 6). Very complicated eruption sequences can also be produced if water is involved and collapse of phreatoplinian eruption columns takes place (Sheridan *et al.* 1981, Self 1983; Fig. 6.33a).

It must be stressed that not all ignimbrite-forming eruptions have an earlier plinian phase, e.g. the Cerro Galan ignimbrite (P. W. Francis *et al.* 1983; Fig. 8.2). This suggests that this very large ignimbrite formed by a rather different eruption mechanism than has been proposed for the well described small- to medium-volume deposits. The mammoth Fish Canyon Tuff, on the other hand, is underlain by a pre-ignimbrite pumice fall deposit and a thick sequence of pyroclastic surge deposits. The implications in terms of type of vent for the very large ignimbrite eruptions is discussed in the next section.

Observations at Mt St Helens have shown that even during small eruptions a high eruption column is not an essential prerequisite for generating a pumice flow (Ch. 5; Fig. 5.12). In such cases the venting eruptive mixture may be so dense that a well defined, maintained eruption column does not form but, instead, a low maintained pyroclastic

fountain, with the appearance of 'a pot boiling over', may form. Another possibility is that rapid lateral expansion of the erupting mixture (exit pressures >1 bar; L. Wilson *et al.* 1980) causes it to move away immediately as a flow.

8.4 Source vents

Several types of source vents for ignimbrites have been proposed. The most voluminous ignimbrites have generally been associated with either linear fissure eruptions (*Valley of Ten Thousand Smokes type* of H. Williams & McBirney 1979) or continuous ring fissure eruptions (*Valles type*). All observed ignimbrite-forming eruptions have issued from what seem to be essentially point sources, or central vents. Studies over the past ten years on a number of smaller- and medium-volume ignimbrites have suggested that these ignimbrites are commonly erupted from central vents.

Ignimbrites are often associated with calderas, a fact which has been recognised for a long time, and was very well documented in the classic paper of H. Williams (1941). Many cases are known where single ignimbrite forming eruptions seem to have resulted in the creation of large calderas (e.g. the Aira caldera in Japan) (Fig. 8.3); Crater Lake, Oregon (Figs 8.16, 13.25 & 26); and Santorini caldera (Figs 8.4, 13.30 & 31)). For example, in the San Juan volcanic field the ignimbrite to caldera ratio is low, suggesting that many eruptions are monogenetic outpourings with each forming a caldera. Figure 8.13 shows that there is a crude relationship between caldera dimensions and the size of the associated ignimbrite. The largest caldera shown is La Garita, which is the source of the Fish Canyon Tuff (Fig. 8.1c). The size of calderas is often assumed to approximate the dimensions of magma chambers at depth. In the case of the San Juan volcanic field each ignimbrite is believed to chronicle the emplacement of successive segments or stocks of an underlying batholith (Steven & Lipman 1976).

Caldera collapse takes place when the lithostatic pressure on the roof of the magma chamber exceeds the chamber pressure by the compressive strength

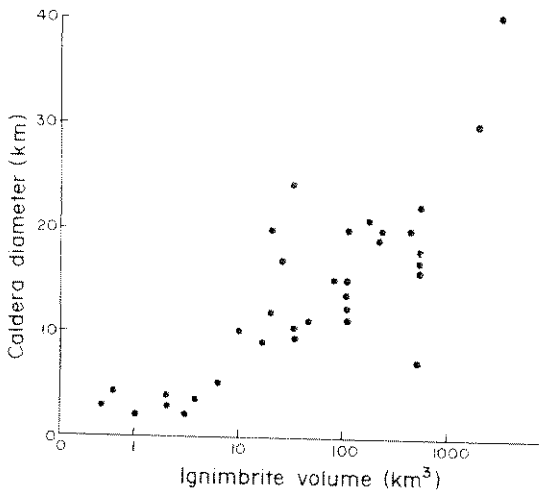

Figure 8.13 Relationship between size of ignimbrite and associated caldera.

of the overlying rock. Whether or not caldera collapse occurs during or after an eruption will be an important control on the type of vent.

8.4.1 LINEAR FISSURE VENTS

The fissure hypothesis originated from the observation of lines of fumaroles in the Valley of Ten Thousand Smokes ignimbrite after the 1912 eruption at Katmai in Alaska (Fig. 8.5). This led C. N. Fenner (1920) to conclude that the ignimbrite erupted from linear fissures in the floor of the valley. However, more recently, from the closure of contours on isopach maps of pyroclastic fall deposits produced in the same eruption, Curtis (1968) located the central vent of Novarupta as the source. The fumarole lines are now thought to be reflections of basement faults along which ground waters moved.

Since Fenner's observations at Katmai, the importance of fissure eruptions for the formation of ignimbrites has been assumed by a number of workers, and has been regarded as the way to account for the more voluminous deposits. Van Bemmelen (1961) considered that ignimbrites were erupted from major fissures in a similar manner to flood basalts. Korringa (1973) documented a linear vent system for the source of the Soldier Meadow Tuff in Nevada, and this is often quoted as an

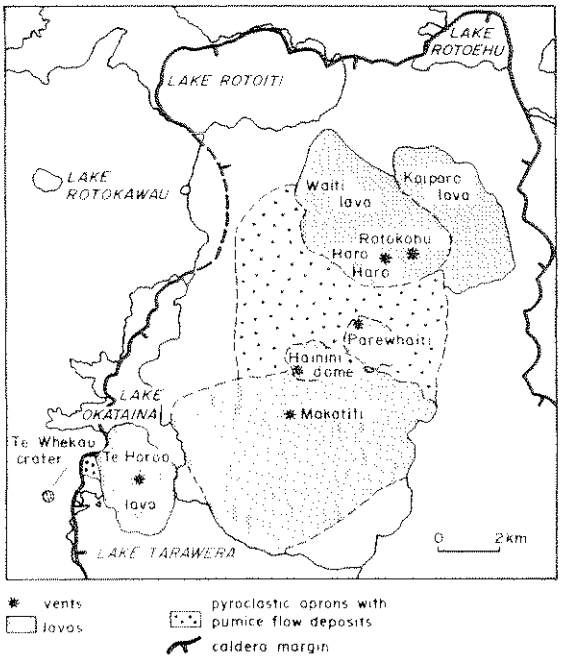

Figure 8.14 Linear fissure vent system of the Mamaku eruption, Okataina rhyolitic centre, New Zealand. (After Nairn 1981.)

example. However, Greene and Plouff (1981) have suggested that this is related to part of the margin of a larger caldera. In many other described examples field evidence for linear fissure vents is meagre or controversial.

Convincing examples are described by Nairn (1981) from the Okataina rhyolitic centre, New Zealand (Ch. 6). All of the post caldera-forming eruptions (<20 000 years BP) are thought to have occurred along fissures from multiple vents in simultaneous or sequential activity. These produced plinian deposits which are interbedded near source with pumice flow and surge deposits and associated lavas, forming thick multiple-bedded deposits. These are exemplified by the Mamaku eruption (7500 years BP), during which at least five magmatic vents and one phreatic vent were active, these being spread along 14 km of an underlying fissure (Fig. 8.14). No major time breaks between the various deposits are apparent, and ^{14}C ages available for two pyroclastic deposits erupted from separate vents are not significantly different. As in basaltic eruptions which begin along fissures, localisation to a number of points seems to have occurred (Chs 4 & 6).

8.4.2 RING FISSURE VENTS

In another popular model ignimbrites are thought to be erupted along a continuous ring fissure, around which caldera collapse may have been occurring during the eruption (R. L. Smith & Bailey 1968). The ring fissure model has been popular in the USA because it explains the radial distribution of thin outflow sheets associated with very much thicker intracaldera ignimbrites, which are thought to have accumulated by ponding of pumice flows erupted around the ring fissure bounding a continually subsiding caldera floor block (Fig. 8.15). However, there have been very few studies that have quantitatively mapped the different facies of larger volume ignimbrites to locate the source vent, as has been done for many smaller-volume ignimbrites.

At Cerro Galan, eruption from around the ring fissure was perhaps the important mechanism throughout. The absence of a pre-ignimbrite plinian deposit could suggest that the radius of the vent widened almost instantaneously. This would make a convecting column unstable, because of the very high eruption rate (Fig. 8.11). P. W. Francis *et al.* (1983) indicated that very large eruption rates would be produced by sinking of the caldera floor block into the magma chamber along outward dipping ring fractures. Inward-dipping ring fractures, as generally suggested in previous models of ring fissure eruptions (Fig. 8.15), would inhibit very high eruption rates. The present thickness of

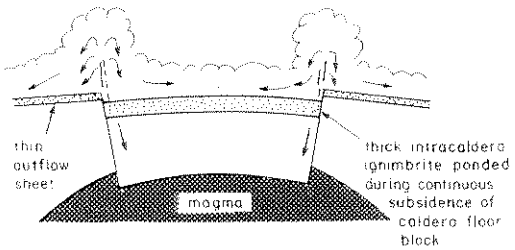

Figure 8.15 The popular ring fissure model for the eruption of ignimbrites.

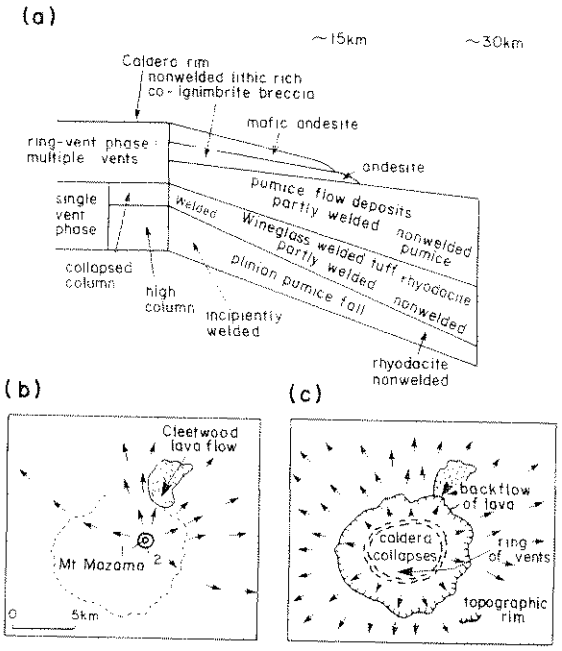

Figure 8.16 (a) Stratigraphic relations and vent type for the products of the 6845 years BP Crater Lake ignimbrite-forming eruption, Oregon. Note also the last erupted pumice flows were mafic andesites in contrast to the earlier rhyodacites, and spectacular compositional zonation is shown. (b) Single vent phase of the eruption; 1 indicates vent for plinian eruption and 2 the enlarged vent during eruption of the pumice flows that deposited the Wineglass welded tuff. Arrows show direction of movement of pumice flows, which were confined to topographic low areas. Mount Mazama is the name given to the pre-collapse stratovolcano. (c) Ring vent phase during which pumice flows surmounted most topographic barriers. The ring fissure is shown inboard of the present topographic rim which would indicate scarp-retreat by landsliding and slumping of the caldera wall during or after caldera-collapse. Field evidence demonstrates the Cleetwood lava flow must have been erupted just before the ignimbrite-forming eruption, and after caldera-collapse backflow down the caldera wall occurred. (After Bacon 1983.)

intracaldera ignimbrite exposed by the resurgent dome is 1200 m (Fig. 8.2), and there is no doubt that caldera collapse must have been concurrent with eruption.

Detailed field studies of the smaller Crater Lake pumice flow deposit have confirmed that eruption from around the ring fracture must have occurred while caldera collapse was taking place (Bacon 1983). The eruption sequence can be divided into two stages: single vent and ring fissure vent phases. The initial plinian phase was erupted from a single vent. Collapse of this column generated a series of pumice flows deposited to the north and east of Mt Mazama (Fig. 8.16). Approximately 30 km^3 of magma was expelled before collapse of the roof of the magma chamber occurred, and the inception of caldera formation ended the single vent phase. Later pumice flows are believed to have erupted from multiple vents around the ring fracture as caldera collapse continued. Composition of lithic clasts within proximal co-ignimbrite breccias (Section 8.5) varies around the rim and certain types can be correlated to probable vent locations. During the ring vent phase another 20 km^3 of magma may have been erupted. Druitt and Sparks (1985) and Druitt (1985) have also proposed such a two-stage model for caldera-related ignimbrite-forming eruptions, based on studies on Santorini.

One noteworthy study of an ancient ring fissure vent system is that by Almond (1971) of the Late-Precambrian–Cambrian Sabaloka cauldron, Sudan. Almond has described welded ignimbrite dykes which he believes fed their eruption around a ring fracture.

8.4.3 VENT SYSTEM FOR THE FISH CANYON TUFF

The eruption sequence of the Fish Canyon Tuff may suggest an alternative type of vent system for the largest ignimbrites (Self & Wright 1983). Where studied, the outflow sheet is underlain by a thin pre-ignimbrite plinian layer, and a relatively thick sequence of pyroclastic beds bounded at the top by a surface having an unusually large wave-like form (Fig. 8.17). These megawaves indicate that there may have been an enormous, sudden release of energy accompanying the eruption. The explanation suggested is that the thin crust over a high-level magma chamber collapsed inwards, effectively opening the magma chamber to the surface and triggering an enormous release of energy, which was translated into lateral blasts or surges. Failure of the roof seems to have occurred soon after the beginning of the eruption, perhaps because the upper part of the magma chamber had

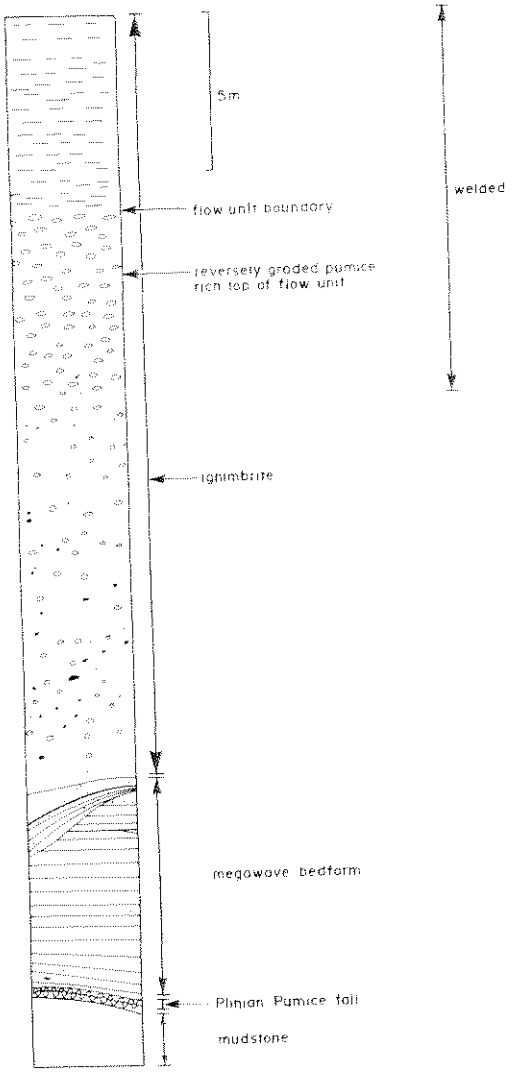

Figure 8.17 Measured stratigraphic section through the outflow sheet of the Fish Canyon Tuff at a location 35 km south-east of the centre of La Garita caldera (Fig. 8.1). (After Self & Wright 1983.)

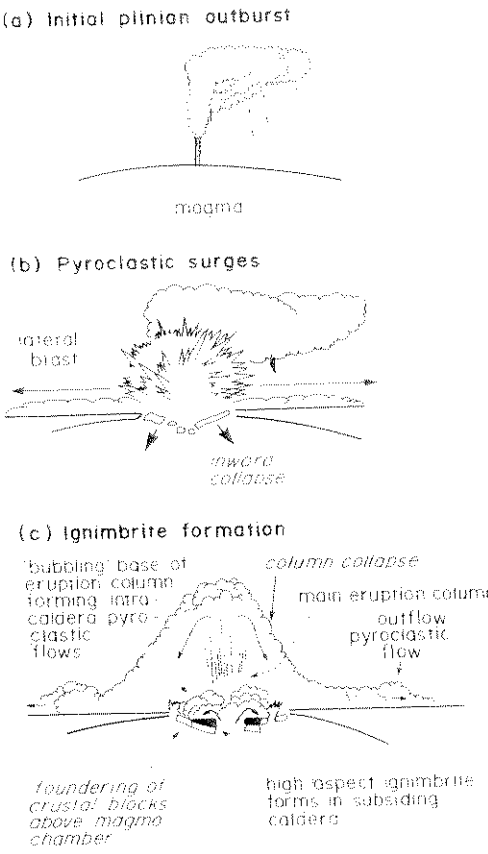

Figure 8.18 Possible eruption sequence for the Fish Canyon Tuff and other very large ignimbrites. (After Self & Wright, *unpubl. data*.)

been quickly drained by a high intensity, initial plinian phase. Figure 8.18 shows schematically the sequence of events. After the surge blasts, the eruption continued to generate ignimbrite-forming pumice flows. As a result of the continued evacuation of magma, failure of the crust over the whole of the present La Garita caldera area may have occurred. Many vents could have opened around foundering crustal blocks over a large area, rather than simply around a ring fracture. It is possible to envisage these being aligned on a complexly organised tensional fracture system and, in a sense, these would be of the linear fissure type. As the eruption continued, more-localised vents may have developed.

With gradual subsidence of crustal blocks into the magma chamber a thick (>1.4 km) intracaldera ignimbrite accumulated. The outflow ignimbrite sheet (20–500 m thick) is composed of a number of flow units, which are similar to smaller volume ignimbrite flow units in their characteristics. The fact that these were able to travel up to 100 km from source suggests they acquired much of their kinetic energy by collapse of a vertical eruption column, probably at least 10 km high. The intracaldera flows (very densely welded and devitrified) could be

more complex in their origin, being composed not only of flows formed by column collapse, but also perhaps generated by frothing over of material at vent without column collapse. Such flows would not be greatly expanded or travel very far, and would build up a thick, high aspect ratio ignimbrite (Section 8.7) within the caldera. Losses of vitric ash should therefore also be minimal. The intracaldera Fish Canyon Tuff, like many other intracaldera ignimbrites, is very crystal-rich, but examination of their juvenile clasts often seems to show that this is a property of the magma, not extreme fractionation by flow processes (Ch. 11).

8.4.4 CENTRAL VENTS

A number of Quaternary ignimbrites have been related to central vents by several methods, including mapping their distribution, mapping the distribution of co-eruptive pumice fall deposits and identifying proximal facies (Section 8.5). These include ignimbrites with associated caldera formation. For example, the Rio Caliente ignimbrite (Fig. 8.31) not only contains a chaotic near-vent facies with co-ignimbrite breccias which can be used to locate a central vent, but also a thicker intracaldera ignimbrite which is partly due to caldera collapse during the eruption. The Minoan eruption sequence has been interpreted in terms of a central vent which progressively widened during the eruption (Fig. 8.11). If this is correct, then caldera collapse, forming Santorini's present caldera, had to happen near the end of or after the Minoan eruption. Similarly, at Krakatau, caldera collapse seems to have taken place very late in the eruption (Self & Rampino 1981). The ultraplinian- and ignimbrite-forming Taupo AD 186 eruption has been related to a central vent. Sudden collapse of the vent area is thought to have greatly widened the vent, and to have triggered the eruption of the violent Taupo ignimbrite, perhaps in a manner somewhat similar to that suggested for the Fish Canyon Tuff, but on a smaller scale and much later in the eruption. Some central vent eruptions have apparently been unrelated to any pre-existing volcano. Just as Paricutin was 'born in a cornfield' in 1943, so the Acatlan ignimbrite was erupted from a 'hole in the ground' vent (located by the near-vent occurrence of a co-ignimbrite breccia and lava dome) on flat ground (J. V. Wright & Walker 1977; see below).

From the foregoing discussion it will be apparent that the vent type and eruption mechanisms for the largest ignimbrites remain unresolved. Models of linear fissure and ring fissure eruptions must be tested by the analysis of eruption sequences and facies, and some of the answers are likely to be found by further examination of ancient volcanic terrains where the roots of large centres and calderas are exposed. Vent type may change as an eruption proceeds (e.g. Druitt 1985). Even if eruption is initiated along a fissure, or if one or more fissures develop due to later caldera-collapse, localisation to multiple vents or a central vent may be a natural progression. During the initial stages of a highly explosive eruption the widest part of the fissure will offer least frictional resistance to the flow of gas and magma. Most-rapid erosion will take place at this point, further accentuating the flow until the eruption is confined to this point. Note that in the theoretical column-collapse models (Figs 8.9, 10, 11 & 6.20) a circular vent is assumed, but the results can be applied to a fissure eruption by replacing the vent radius with the half-width of the fissure.

8.5 Co-ignimbrite breccias

Proximal ignimbrite breccias generated in the eruption column and as part of an ignimbrite are now known to be common. J. V. Wright and Walker (1977) first described a co-ignimbrite lag-fall deposit from the Acatlan ignimbrite (Fig. 8.19). This coarse, lithic-rich deposit was identified as part of the ignimbrite because it showed the same compositional zoning as the ignimbrite (Figs 7.19 & 20). This was the key to the interpretation, because it showed that the breccia accumulated synchronously with the formation of the ignimbrite, together possibly representing only one flow unit. J. V. Wright and Walker (1977, 1981) envisaged that the deposit formed at or near the site of continuous column collapse, and consisted mainly of pyroclasts

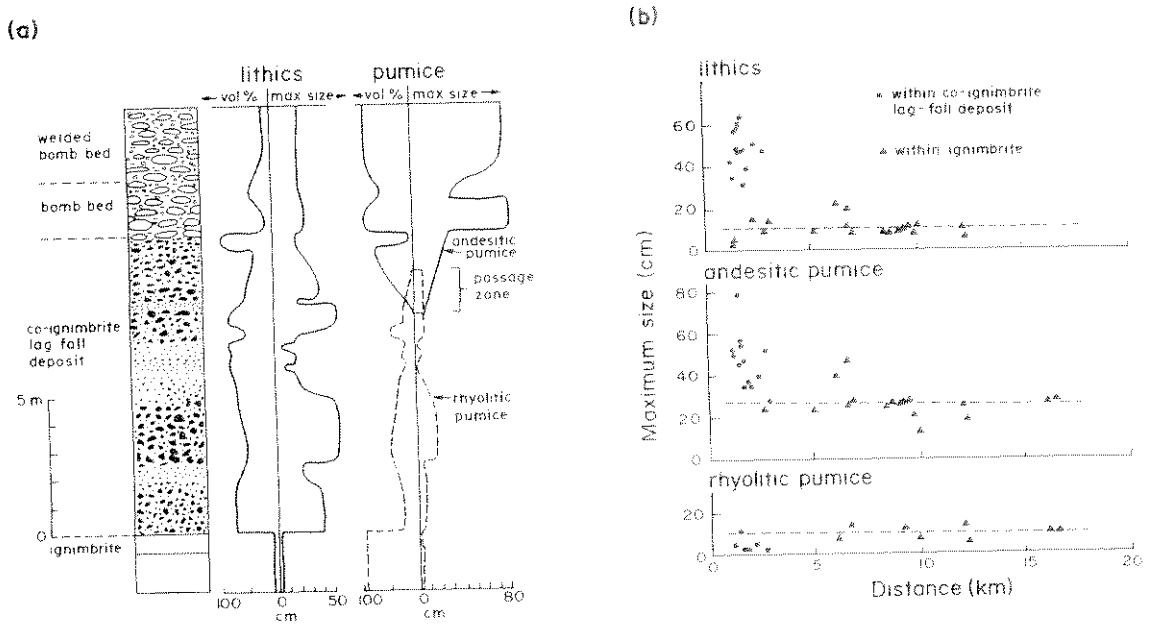

Figure 8.19 (a) Measured stratigraphic section through the Acatlan lag-fall deposit, Mexico, approximately 1.5 km from the most likely source vent; the conduit now covered by a rhyolite lava dome. (b) Average maximum diameter of the five largest clasts plotted against distance from source in the main, compositionally zoned ignimbrite flow unit and the lagfall deposit. (After J. V. Wright & Walker 1977.)

that were too large and heavy for the column to support. The term *'lag-fall'* deposit was proposed, because the accumulation of lithics was a residue left behind by the pumice flows – that is, a lag deposit. The lag deposit was of air-fall type as shown by the stratification. The absence of fine-grained fall units (ash grade <2 mm) and of discrete bedding planes was thought to be evidence for rapid accumulation from a continuous, vigorous eruption column with only minor variations in eruption intensity.

Similar breccias have since been recognised as a near-vent facies of several ignimbrites (Figs 8.20 & 21). However, it is now realised that there are different types, and a better general term to use for these rocks is simply co-ignimbrite breccia. Many of these examples did not simply accumulate by the fall of lithics out of the eruption column, as originally envisaged for the Acatlan ignimbrite, but were emplaced by flow processes. Such types of deposit include clast-supported lithic breccias containing a small amount of ignimbrite matrix. In some cases they may grade into matrix-supported breccias and coarse pumiceous ignimbrite containing large lithics (Figs 8.21 & 22). These deposits can contain large segregation pipes and structures enriched in lithics and depleted in fines, which indicate a high degree of fluidisation in the proximal pumice flows (Ch. 7). Complex interrelations between breccias and ignimbrite can be found (Fig. 8.21).

Recent work shows that there are two types of proximal ignimbrite breccias emplaced by flow. In the first type, segregation of lithics takes place through the body of the flow, and this is found above a basal layer. This type is the near-vent equivalent of the lithic concentration zone commonly observed at the bottom of layer 2b in ignimbrite flow units (Ch. 7). Towards the vent this type of breccia should grade back into a co-ignimbrite lag-fall of the Acatlan-type, in which lithics settled out of the eruption column. Druitt and Sparks (1982) have logically proposed that both these cases of body segregation breccias should be termed co-ignimbrite lag breccias. In the second type, the segregation of lithics appears to have

Figure 8.20 Examples of co-ignimbrite breccias. (a) The Kamewarizaka breccia, a proximal facies of the Ito pyroclastic flow deposit found close to the edge of Aira caldera, Japan (Fig. 8.3). Largest lithics are 20–30 cm in diameter. Lighter coloured lower half is the older Tsumaya pyroclastic flow deposit (photograph by S. Yokoyama). (b) Lag breccia in the Rio Caliente ignimbrite, Mexico. Note segregation pipes. Largest lithic is a block of welded Rio Caliente ignimbrite which has been *erupted*, indicating considerable vent widening or migration during the eruption. (c) Lag-breccia of the 18 500 years BP eruption of Santorini, Greece (Fig. 13.31). The breccias overlie a basal plinian pumice fall deposit (against which the geologist is resting his hand) and show normal grading (after Druitt & Sparks 1982). (d) Lenticular segregation pod in lag breccias of the 18 500 years BP Santorini eruption (photograph by T. H. Druitt).

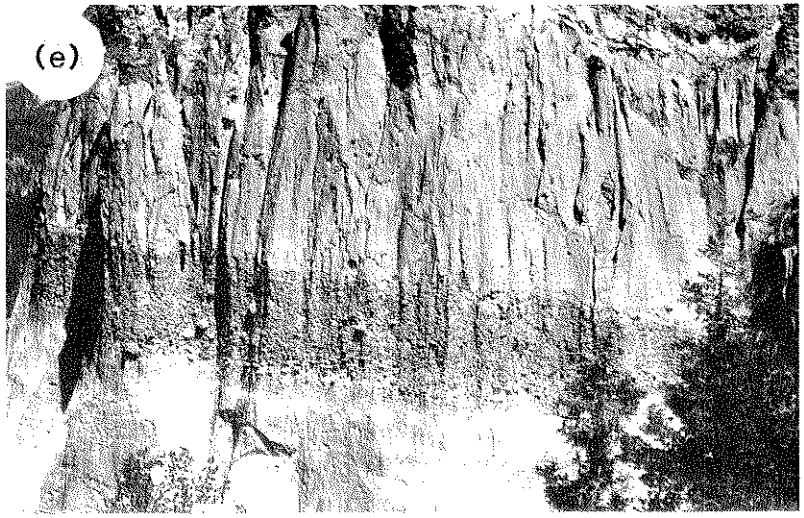

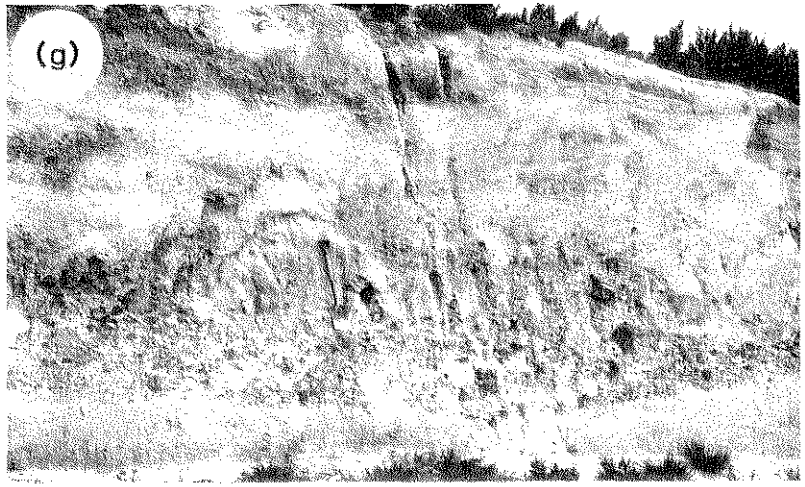

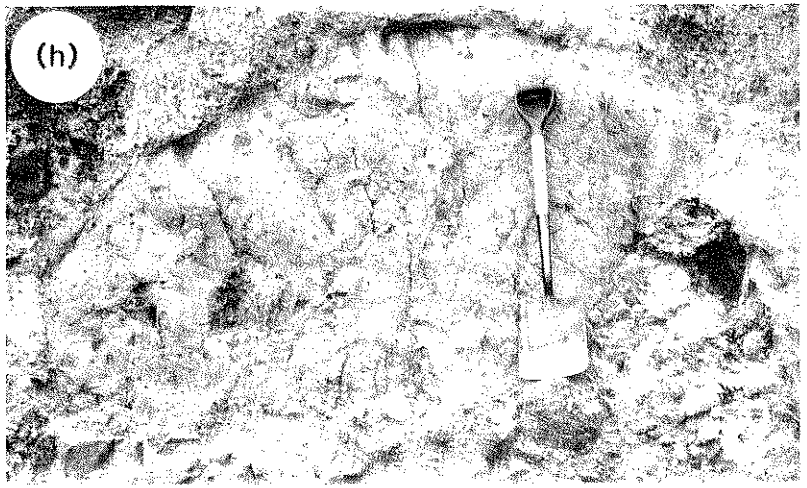

Figure 8.20 *continued*
ignimbrite breccia bed in the Lower Bandelier Tuff, New Mexico. (f) Close-up of Lower Bandelier co-ignimbrite breccia showing largest clasts up to nearly 2 m. (g) Ground breccia of the Taupo ignimbrite at a location approximately 8 km from the vent, New Zealand. The base of the ground breccia is sharply erosional, here it overlies a local early ignimbrite flow unit (Section 8.12). (h) Detail of the Taupo ground breccia with large, well rounded mudstone block. Spade is in same position seen in (g).

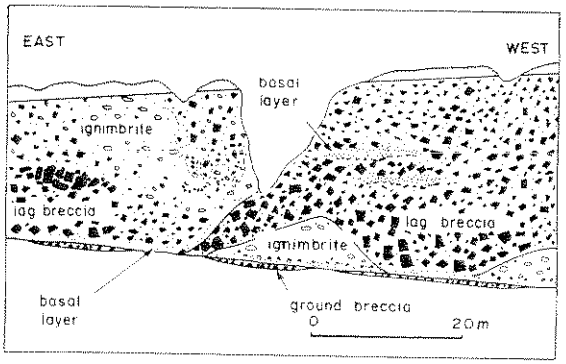

Figure 8.21 Field sketch at an exposure in the Santorini caldera wall showing co-ignimbrite breccias of the 18 500 years BP eruption, Santorini, Greece. This illustrates the complex relationships that can be found between such proximal breccias and ignimbrite. (After Druitt & Sparks 1982.)

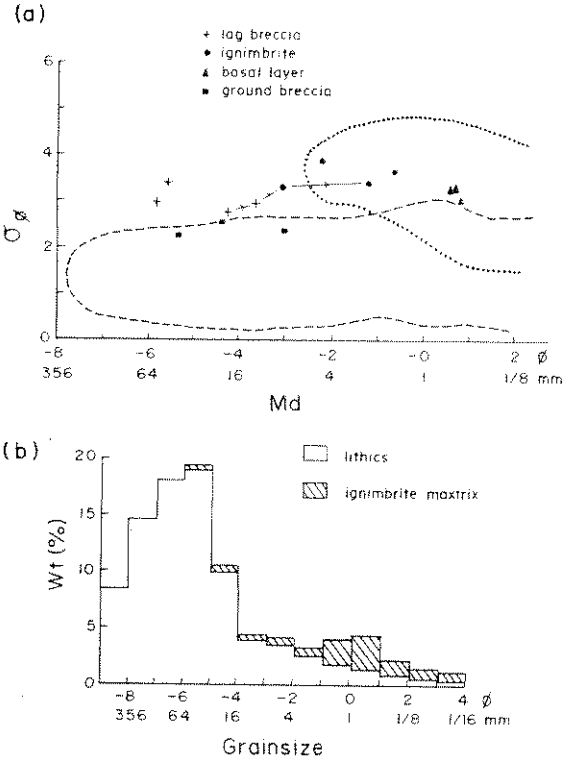

Figure 8.22 (a) Md_ϕ/σ_ϕ plot for proximal deposits of the Santorini 18 500 years BP eruption, Greece. Tie-lines with arrows connect samples taken from a gradational section measured on the eastern side of location sketched in Figure 8.21. (b) Grainsize histograms of a typical lag-breccia. The deposit is bimodal with a mode in the >0.5 mm fraction due to a high proportion of crystals. (After Druitt & Sparks 1982.)

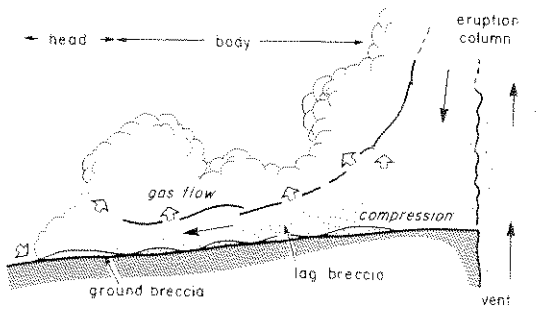

Figure 8.23 Model for the proximal segregation of lithic clasts in pumice flows generated by column-collapse. Ingestion of air at the flow-head causes strong fluidisation, and the sedimentation of the ground breccia. Compression of the particle-gas mixture at the base of the collapsing column generates high pore pressures within a high particle concentration flow body. Decompression of the gas phase as the flow moves away laterally causes strong fluidisation within the body, and the segregation of lithics to generate the lag breccia. Open arrows schematically depict the passage of gas through the flow system. (After Druitt & Sparks 1982.)

taken place in the more strongly fluidised head of the moving pumice flow. This layer is then overridden by the rest or body of the flow (with layers 2a and 2b). This type has been termed a **ground breccia**, and the best example that has been described is associated with the Taupo ignimbrite (Figs 8.20g & h). This is the proximal equivalent of the ground layer (G. P. L. Walker *et al.* 1981a; Ch. 7). Both types of breccia can be found within the same flow unit. For their formation, Druitt and Sparks (1982) have suggested the model illustrated in Figure 8.23. Druitt (1985) has suggested that the sudden appearance of lag breccias between normal ignimbrites above and below, on Santorini, records the change from a single point source eruption point to caldera collapse. This leads to an increased discharge rate, erosion of the collapsing roof materials and eruption of the eroded blocks together with ignimbrite from multiple eruption points along the caldera collapse fracture system, as multiple, localised deposits of lag breccia. The succeeding normal ignimbrite records a return to a single, stable eruption point.

Other types of breccia may be generated during eruption of ignimbrites and are found closely associated with them near vent. Lipman (1976) has

Figure 8.20 *continued*
ignimbrite breccia bed in the Lower Bandelier Tuff, New Mexico. (f) Close up of Lower Bandelier co-ignimbrite breccia showing largest clasts up to nearly 2 m. (g) Ground breccia of the Taupo ignimbrite at a location approximately 8 km from the vent, New Zealand. The base of the ground breccia is sharply erosional, here it overlies a local early ignimbrite flow unit (Section 8.12). (h) Detail of the Taupo ground breccia with large, well rounded mudstone block. Spade is in same position seen in (g).

described caldera-collapse breccias within intracaldera ignimbrites in the San Juan volcanic field as meggabreccias including clasts metres to hundreds of metres in size (e.g. Thompson 1985). These are thought to have formed by landslides from the walls of calderas as collapse took place (see caption to Fig. 8.16c and Ch. 13). Flash-flood breccias are a prominent feature of the Minoan ignimbrite (Bond & Sparks 1976; Fig. 7.15). G. P. L. Walker (1985) has comprehensively reviewed the origin of coarse lithic breccias near ignimbrite source vents.

8.6 Co-ignimbrite ash falls

In recent years it has become apparent that large-volume ignimbrites should have associated with them large and very widespread air-fall ashes which are synchronous with emplacement of the ignimbrite (Ch. 5). Ignimbrites commonly show a marked concentration of free crystals in the matrix compared with the juvenile magmatic content. This may be attributed to the large amount of vitric dust that has been lost during eruption and pyroclastic flow, and is then deposited in an associated co-ignimbrite ash-fall deposit (Sparks & Walker 1977; Chs 5 & 11). From crystal concentration studies (App. I), ignimbrites show average vitric ash losses of at least 35% from the total erupted magma. Thus, for an ignimbrite having a volume of 200 km^3, there may be more than another 100 km^3 accompanying this as widely dispersed air-fall ash.

The significance of co-ignimbrite ashes is even greater when the volumes of plinian deposits are considered. Very few plinian deposits are known to be greater than 25 km^3 in volume (Table 6.2). Although dispersal is not necessarily related to volume, this at least shows that extensive, very widely dispersed volcanic ashes are more likely to be associated with the formation of the ignimbrite, rather than with a preceding plinian phase or individual plinian eruptions. However, the volcanological interpretation of distal silicic air-fall ash layers is not easy. Other types of eruption will produce widely dispersed ash layers, and the plinian component can be substantial (Ch. 6).

During the eruption of ignimbrites, two sources from which fine ash could be carried high as convective plumes are (a) above the collapsing column and (b) above the moving pyroclastic flow.

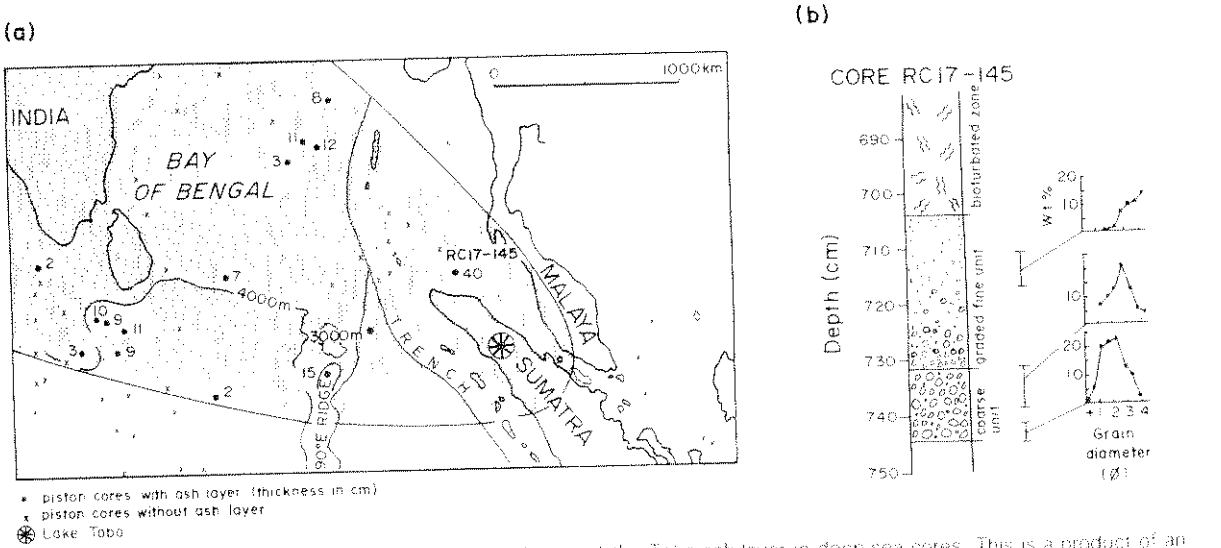

Figure 8.24 (a) Map showing the distribution and thickness of the Toba ash-layer in deep-sea cores. This is a product of an eruption from Lake Toba, Sumatra, 75 000 years BP, which produced a 2000 km^3 ignimbrite (Table 8.1), and is the largest magnitude eruption documented in the Quaternary. (b) Section showing the ash layer in the most proximal core. The lower, coarser unit is interpreted as a distal plinian ash, and the upper graded fine unit the co-ignimbrite ash. (After Ninkovich *et al.* 1978.)

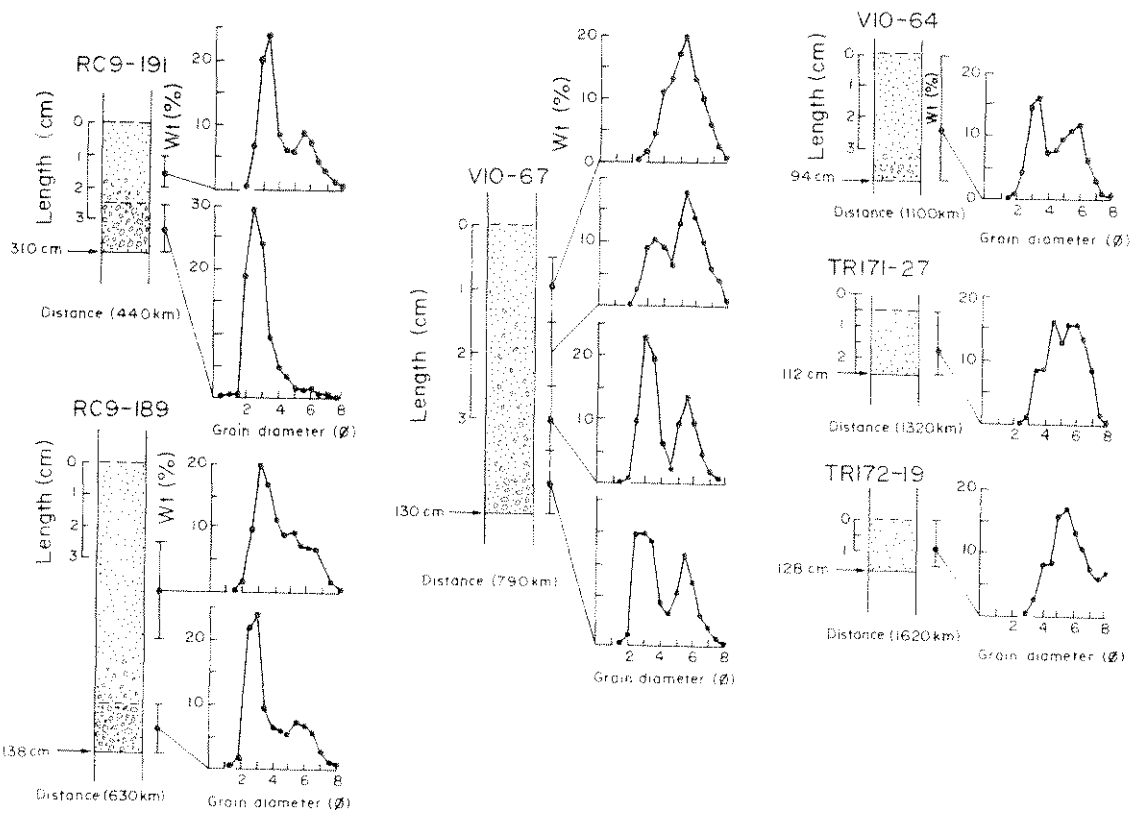

Figure 8.25 Sections showing the Campanian (Y-5) ash layer in six deep-sea cores from the eastern Mediterranean Sea at increasing distance from the Bay of Naples. This is correlated with the Campanian ignimbrite, distributed over a large area in the Neapolitan region (Table 8.1, Ch. 13). (After Sparks & Huang 1980.)

When pyroclastic flows are generated by column collapse a convective column rises above the vent, producing a high eruption column, and lower clouds of fine ash rise above the moving pumice flows (Fig. 8.8). It is the preferential loss of vitric material into convecting plumes which leads to a complementary increase in the proportion of crystals in the ignimbrite. Sparks *et al.* (*in press*) have also suggested that some flows may become completely buoyant at their distal flow margins, and then rise into the atmosphere producing a major mushroom-like plume of ash. This may be the source of very large volumes of co-ignimbrite air-fall deposits. This work is based on analysis of space and ground photographs of the 18 May 1980 Mt St Helens blast event, which suggests the growth and rise of a major ash cloud at a point well away from the vent.

Many of the volcanic ashes found in deep-sea cores are considered to be co-ignimbrite ash layers (e.g. Figs 8.24 & 25). The largest known is that associated with the Toba Tuff, erupted from Lake Toba, Sumatra. Nearer to the source, cores also pick up the distal plinian ash below the co-ignimbrite ash; in all the described examples this is a thinner, coarser layer which peters out with distance. In more-proximal cores through the Campanian ash layer of the eastern Mediterranean (Fig. 8.25), this ash is clearly divisible into a coarse lower unit separated by a sharp boundary from a fine graded upper unit. In core RC9-191 the lower unit only shows a coarse mode, whereas the normally graded top possesses a coarse and a finer mode. The normally graded unit in core V10-67 has a bimodal distribution throughout most of its thickness. Bimodality disappears downwind, because the coarser mode decreases in diameter

with distance from source, but the finer mode shows no lateral variation. During the plinian phase of an eruption the coarse-grained lower unit, and at least part of the coarse mode found in bimodal ashes, is formed. The fine-grained upper unit is the co-ignimbrite ash. The higher convecting plume above the collapsing column may also contribute to the coarse mode in this layer. However, bimodality in distal silicic ash layers is not unique to co-ignimbrite ashes and can be produced by other mechanisms (Ch. 6). Observations on the size grading of crystals in deep ash layers are also important, and can be used to estimate eruption durations (Ch. 9).

In the geological record, many of the stratigraphically important bentonite layers and 'tonsteins' may be co-ignimbrite ashes, perhaps derived from late stage, buoyant plumes originating from the distal margins of flows as suggested by J. G. Moore *et al. (in press)*.

8.7 Depositional facies model

For our purpose here, a *facies* can be considered as an eruptive unit, or part thereof, having distinct spatial and geometrical relations and internal characteristics (e.g. grainsize and depositional structures; Ch. 1). A *facies model* is a generalised summary of the organisation and associations of the facies in space and time.

C. J. N. Wilson and Walker (1982) described the different facies that could be found in an ignimbrite and related them to the depositional regimes or 'anatomy', of the moving pyroclastic flow. However, much of this discussion was based on the study of one ignimbrite – the excellently preserved Taupo ignimbrite. This has exceptionally well developed facies contrasts, related to the extreme '*violence*' or velocity with which it was emplaced (Ch. 7). Indeed, the Taupo ignimbrite can be considered to be at one end of a spectrum of ignimbrite types. Ideally, when constructing facies models of depositional systems it is important to study many examples. It is only after the local effects of a number of examples are '*distilled away*' that a generalised model results (Ch. 14). However, unlike many sedimentary systems, there are still relatively few ignimbrites for which different facies and lateral relationships are known. One example where lateral relationships have been evaluated are in the Laacher See tephra in Germany, where Freundt and Schmincke (1985) have been able to identify proximal, medial and distal facies.

The model presented here is largely developed from a study of the Bandelier Tuffs (J. V. Wright *et al.* 1981). Seminal works on many of the characteristics of ignimbrite volcanism originated from studies of these deposits (R. L. Smith 1960a, b, Ross & Smith 1961, R. L. Smith & Bailey 1966, 1968). The Bandelier Tuffs are therefore already models for this type of volcanism, and we consider them to be a good norm for comparison, which is an important property of any facies model (R. G. Walker 1984; Ch. 14). To illustrate the extremes in ignimbrites, we can also examine and compare the Rio Caliente and Taupo ignimbrites, which seem to be at the opposite ends of the spectrum of ignimbrite types. Readers are also referred to the facies model of Freundt and Schmincke (1985) for ignimbrites of the Laacher See volcano in Germany.

8.7.1 BANDELIER TUFFS AND MODEL

The Lower and Upper Bandelier tuffs of New Mexico are the products of two voluminous, rhyolitic ignimbrite-forming eruptions, dated 1.4 and 1.1 Ma BP, respectively. Associated with these eruptions was the formation of a large caldera complex, including the Valles caldera and the Toledo caldera (Figs 8.26, 13.42 & Plate 13). Toledo caldera was believed to be the source of the earlier ignimbrite, and Valles to be that of the later ignimbrite. Stratigraphically the Lower and Upper Bandelier tuffs are separated by erosional surfaces, epiclastic sediments, soils and a sequence of up to six pumice-fall (sub-plinian or plinian) deposits (Plate 8) erupted from rhyolite domes in Toledo caldera.

Both tuffs have similar eruption histories. Extensive plinian fall layers occur at their bases (Plate 8, Figs 6.13b, 14a & b). The Lower Bandelier plinian deposit with its volume of 100 km^3 and the Upper plinian deposit with its volume of 70 km^3

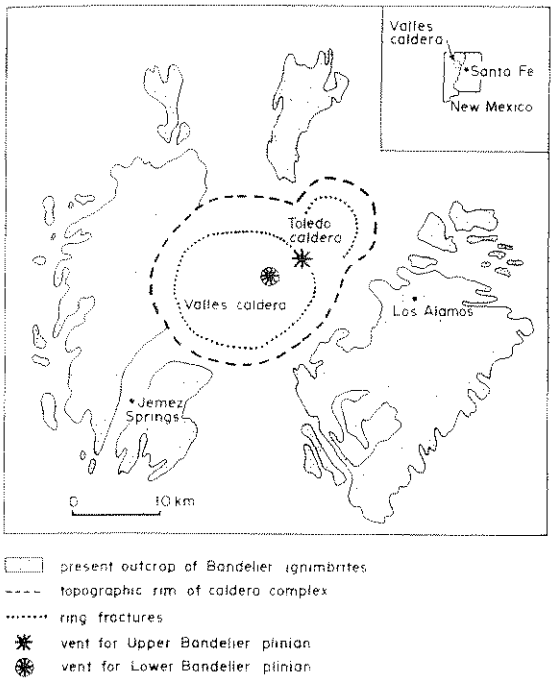

Figure 8.26 Location map of the Bandelier Tuffs, New Mexico. Vent positions are from Self & Wright (*unpubl. data*).

are two of the most voluminous yet recognised (Ch. 6). Each has a lower, thick, homogeneous fall unit, produced by the continuous gas-blast of a high intensity, maintained, stable eruption column. The homogeneous units are overlain by finely bedded fall units, which are locally interstratified with pyroclastic surge and flow deposits. These are indicative of instabilities in the column, documenting fluctuations in gas exit velocity, mass discharge rate, column height and minor collapse events. Dispersal patterns of fall units within the plinian deposits indicate the location of a central vent for each eruption (Fig. 8.26). The sequence of deposits suggests a continuum of events leading to a major collapse (Fig. 8.11). Also, the initial pumice flows at least seem likely to have been erupted from the same central vents. Eruptions along a ring-fissure vent system may have developed later.

The two ignimbrites both have volumes of about 200 km^3, and consist of a number of flow units. Flow unit thickness varies from <1 m to >20 m, although in some of the deep palaeocanyons where the ignimbrites are ponded and densely welded (see Fig. 8.42, below), individual flow units could have had uncompacted thicknesses of more than 100 m. For most of the two sheets, any one section only shows a small number (two to four) of massive flow units (Plate 8). Basal layers, normal grading of lithic clasts and reverse-grading of pumices are often evident.

Lithic breccias are interbedded, and grade into ignimbrite flow units in the caldera wall. These are co-ignimbrite lag breccias. The breccias form thick segregation layers (Figs 8.20e & f), segregation pods and large pipes. The appearance of lag breccias associated with the ignimbrites of the caldera wall may herald the onset of caldera collapse and the opening of ring fracture vents.

The ignimbrites are underlain by ground surge deposits (Plate 8, Figs 5.23a & b) and we have already discussed the possibilities for the generation of this facies (Chs 5 & 7). Also, directly below the base of the lowermost flow unit of the Lower Bandelier ignimbrite, large pumice clasts occur in dune bed-forms (height 0.5–1.5 m, wavelength 5–10 m; Fig. 8.27) and in discontinuous lenses (*pumice swarms*). These pumice swarms have also been found in the thin flow units at the base of the Upper Bandelier ignimbrite. More rarely, such pumice concentrations have been found at the base

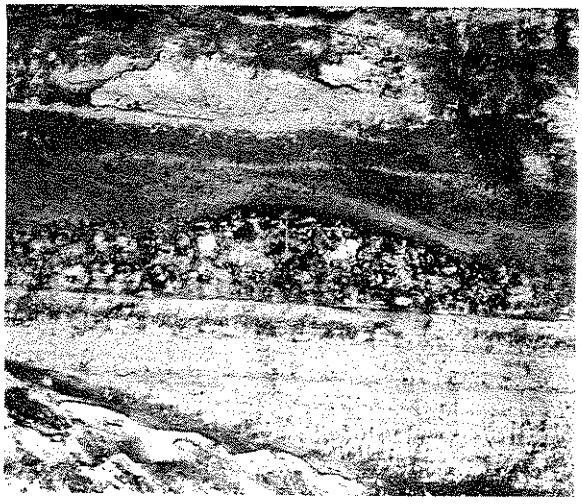

Figure 8.27 Pumice dune below base of lowermost flow unit of the Lower Bandelier ignimbrite. Height of crest is 50 cm.

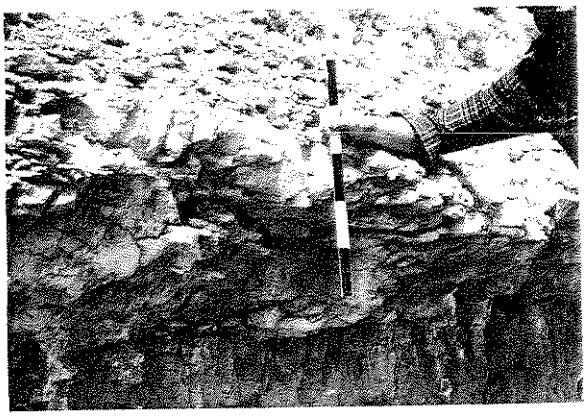

Figure 8.28 Thin, very pumice-rich, reversely graded flow units and ash-cloud surge forming a distal facies association of the Upper Bandelier ignimbrite. Deposits are indurated by vapour-phase crystallisation (Section 8.10)

of flow units higher up in the ignimbrites, but they are certainly best developed in the lowermost one. They represent jets of turbulent, highly fluidised material which burst forward from the flow-head (Ch. 7). This process was best developed in the initial pumice flow because its flow-head was ingesting cold air which would greatly expand, enhancing fluidisation. Later flows ingested considerably hotter, and probably ash-charged, air which would expand less.

Ground- and ash-cloud surge deposits also occur interbedded with ignimbrite flow units (Figs 5.23c & d). Ash-cloud surge deposits of the Upper Bandelier ignimbrite have been described by Fisher (1979). These are best developed at the edge of the ignimbrite sheet associated with a number of relatively thin, very pumice-rich, reversely graded flow units (Fig. 8.28). These features suggest that, distally, pumice flows were splitting up into separate lobes, ash-cloud surges were well developed and pumice was being dumped at the flow-fronts. These processes are also all recognised at Mt St Helens, but on a different scale.

Fine-grained ash from the eruption of the Lower Bandelier Tuff is known to have been dispersed 500 km (Fig. 8.29). This distal ash deposit is divisible into two layers. There is a lower, coarser ($Md\phi$ = 2.9), crystal-rich (36 wt% free crystals) layer and this is regarded as distal Lower Bandelier plinian fall. An upper, finer-grained ($Md\phi$ = 4.1), vitric (14 wt% free crystals) layer is regarded as a co-ignimbrite ash fall. Crystal concentration studies of the Lower Bandelier ignimbrite show that approximately 100 km^3 of ash should have been deposited as a co-ignimbrite ash-fall, and for the Upper Bandelier ignimbrite one of comparable volume is indicated.

In Figure 8.30 the different depositional facies are placed together schematically as a model for the products of ignimbrite-forming eruptions.

8.7.2 RIO CALIENTE AND TAUPO IGNIMBRITES

Both of these ignimbrites have vesiculated volumes of about 30 km^3, which makes them an order of magnitude smaller than each of the Bandelier ignimbrites. The Rio Caliente ignimbrite, from Mexico, was formed from a low intensity (low magma discharge rate) eruption, forming a multiple-flow unit deposit (Fig. 5.16a) with a high aspect ratio (1 : 300) (J. V. Wright 1981). At the other end of the spectrum, the Taupo ignimbrite, from New Zealand, was erupted with an extremely high magma discharge rate and travelled with an extremely high velocity. It formed a low-aspect ratio (1 : 70 000) ignimbrite, consisting of a single-flow unit, and travelled radially outwards in all directions, almost regardless of topography, climbing

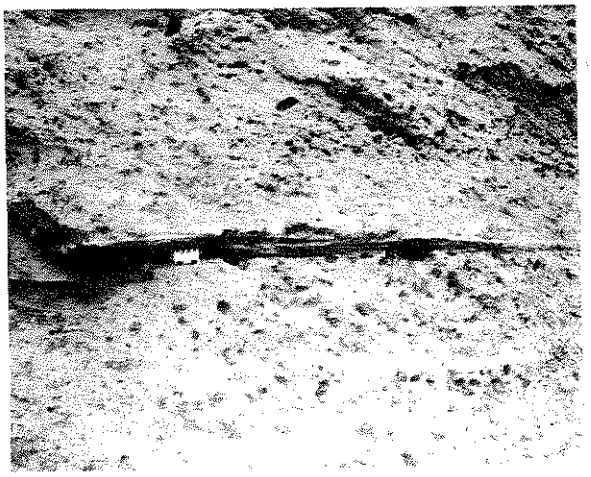

Figure 8.29 Distal air-fall ash layer from the Lower Bandelier eruption at Floydada, Texas.

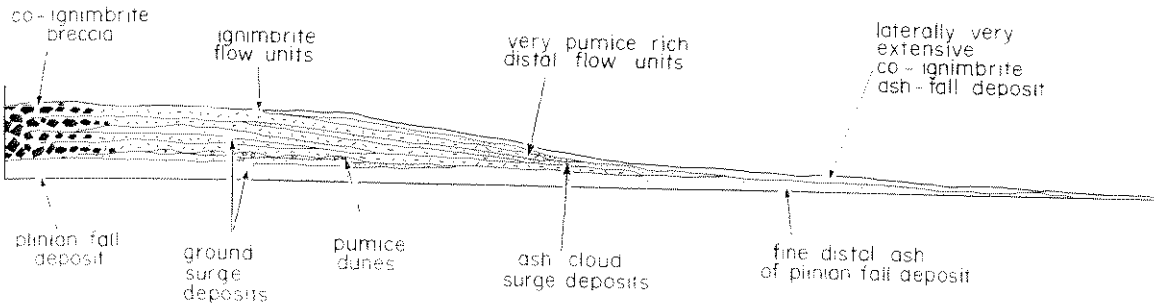

Figure 8.30 Depositional facies model for the products of ignimbrite-forming eruptions based on the Bandelier Tuffs. (After J. V. Wright *et al.* 1981.)

hills up to 1500 m above the vent in Lake Taupo (Ch. 7).

Maps of the two ignimbrites are shown in Figures 8.31 and 32. The distribution of facies in the Taupo ignimbrite is strikingly different from those in the Rio Caliente ignimbrite and our Bandelier Tuff model. Several important differences can be highlighted:

(a) An outstanding feature of the Taupo ignimbrite is that it occurs in two contrasting forms, each having quite different relationships to the pre-existing land surface. One is a landscape mantling ignimbrite veneer deposit (IVD), while the other fills in depressions like 'conventional' ignimbrites do, and is called valley-ponded ignimbrite (VPI; Figs 8.32a & 7.27). The IVD is stratified and occasionally shows bedforms. All of the evidence suggests this was left behind as a 'trail-marker' by the rapidly moving Taupo flow (Ch. 7). Such types of layers have not been found in the less mobile Rio Caliente ignimbrite, which is composed of normal flow units. However, the Rio Caliente ignimbrite seems to have been erupted onto gentle topography, and if hills were present maybe local ignimbrite veneer deposits could have formed; such a local veneer deposit has been found at one locality in the Upper Bandelier ignimbrite. What is important is they could never have been an important facies, as in the Taupo ignimbrite.

(b) Co-ignimbrite breccias in the Taupo ignimbrite extend much further from the vent. They are of the ground breccia type, generated in the extremely fluidised head of the Taupo flow. Laterally they pass into the Taupo ground layer and the >10 cm average

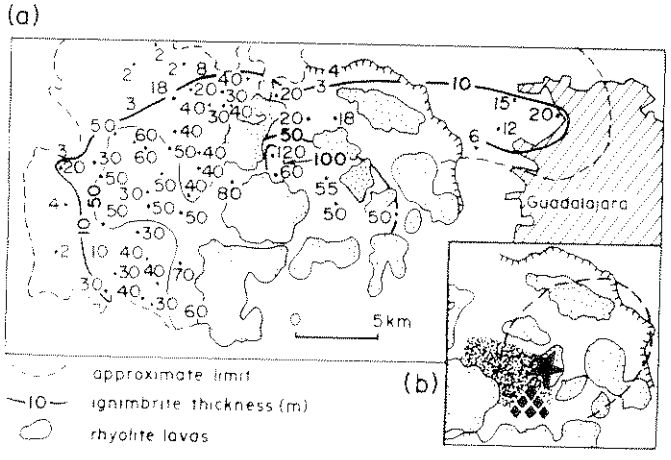

Figure 8.31 (a) Isopach map of the Rio Caliente ignimbrite, Sierra La Primavera volcano. The base of the ignimbrite is rarely seen and so recorded values are minimum values. Within the caldera area (Ch. 13) the ignimbrite is now known from drilling to be as much as 360 m thick, suggesting that caldera-collapse was also concomitant with the eruption. (b) Location of vent position (star); solid diamonds represent exposed proximal ignimbrite facies with co-ignimbrite breccias and fines-depleted ignimbrite; broken line is >1 m lithic isopleth for the co-eruptive plinian fall (Fig. 8.12). Also shown is the distribution (close stipple) of some localised mixed-pumice flow units which travelled only a short distance from the vent. (After J. V. Wright 1981.)

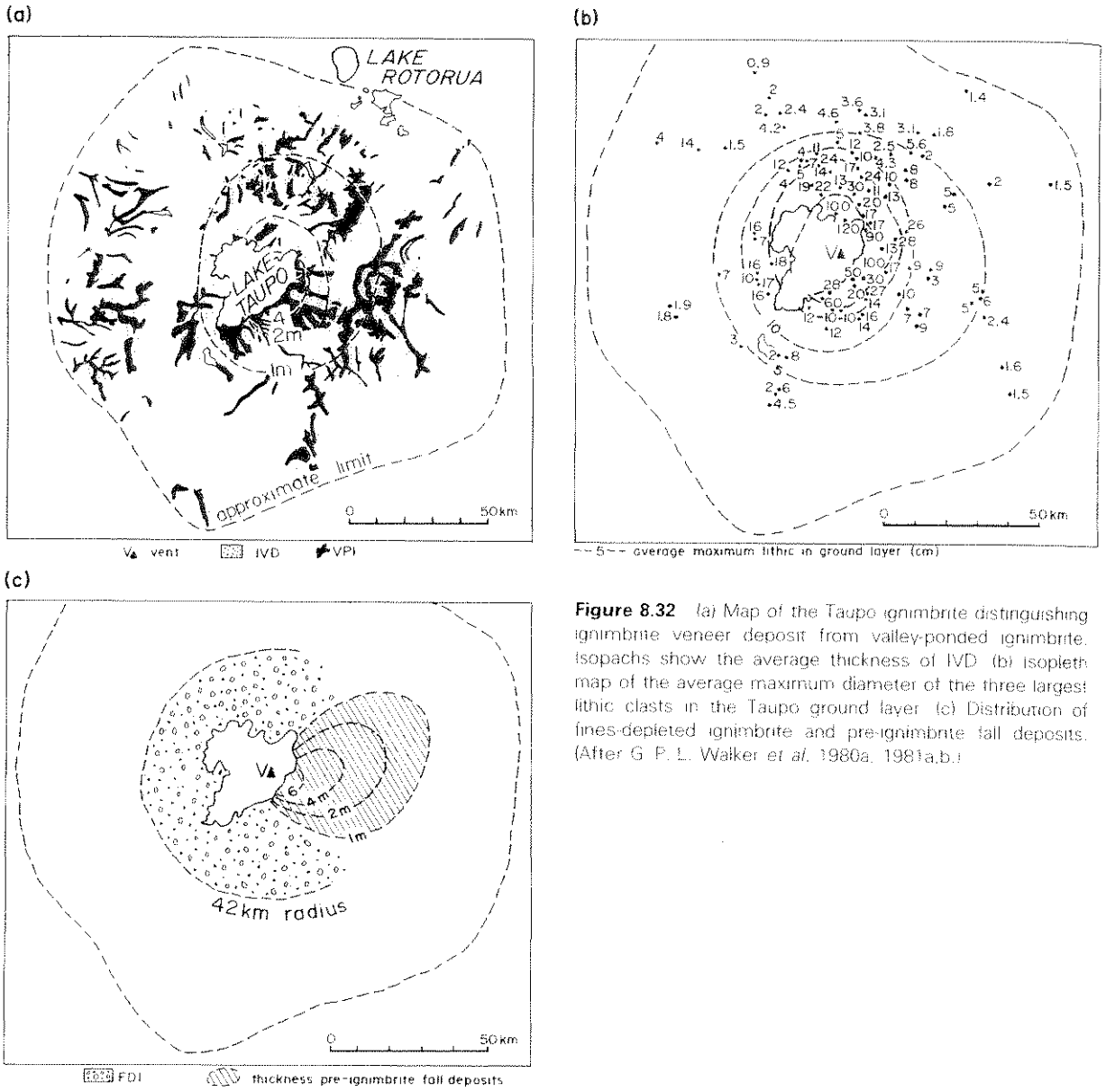

Figure 8.32 (a) Map of the Taupo ignimbrite distinguishing ignimbrite veneer deposit from valley-ponded ignimbrite. Isopachs show the average thickness of IVD. (b) Isopleth map of the average maximum diameter of the three largest lithic clasts in the Taupo ground layer. (c) Distribution of fines-depleted ignimbrite and pre-ignimbrite fall deposits. (After G. P. L. Walker *et al.* 1980a, 1981a,b.)

maximum lithic size isopleth extends 35 km approximately radially around the vent (Fig. 8.32b). The co-ignimbrite breccias identified in the Rio Caliente ignimbrite (Fig. 8.31b) formed by segregation through the bodies of proximal pumice flows, and are of the lag breccia type. These only extend up to a maximum of 4 km from the vent. No ground breccias have been found in the Rio Caliente ignimbrite.

(c) Another quite remarkable facies of the Taupo ignimbrite is fines depleted ignimbrite (FDI). This is very distinctive in the field, and is characterised by large rounded framework pumice clasts, with few fines and abundant charcoal fragments (Fig. 7.28). The FDI is

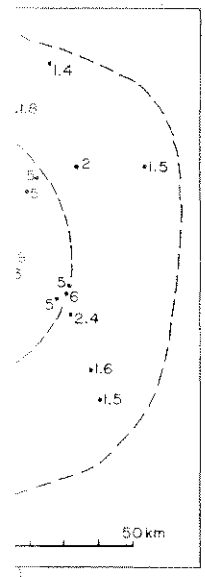

onte distinguishing
onded ignimbrite.
IVD. (b) Isopleth
the three largest
(c) Distribution of
nte fall deposits.
(c))

he Rio Caliente

es of the Taupo
nimbrite (FDI).
ne field, and is
ded framework
and abundant
). The FDI is

restricted to an area where vegetation was not covered by earlier co-eruptive fall deposits (Fig. 8.32c; Section 8.12). The FDI is thought to be material jetted out *en masse* from the flow head (similar to the pumice dunes), but in this case mixed with large amounts of vegetation which also generated large amounts of gas, carrying off even more fines. This fines depleted facies extends 42 km from the vent. Ignimbrite depleted in fines is found in the Rio Caliente ignimbrite, but this only occurs in proximal locations closely associated with co-ignimbrite breccias (Fig. 8.31b). This is again a facies consistent with a high degree of agitation–fluidisation near the vent in proximal pumice flows, as they are segregating from the collapsing column.

(d) Following on from the above, total loss of vitric material is very much greater in the Taupo ignimbrite than the Rio Caliente ignimbrite. Although both ignimbrites have similar volumes, the quantity of ash occurring as a co-ignimbrite ash-fall facies is quite different for each. The Taupo co-ignimbrite ash has an estimated volume of 20 km^3 and the Rio Caliente co-ignimbrite ash only 7 km^3. This was clearly controlled by the degree of expansion and mobility of the moving pumice flows (Section 7.3).

8.7.3 IGNIMBRITE FACIES AND ERUPTION RATE

The most important control on the overall geometry and internal characteristics, and therefore facies, of the Rio Caliente and Taupo ignimbrites is believed to be magma discharge rate. J. V. Wright (1981) drew the analogy between multiple and single flow unit ignimbrites, and compound and simple lava flows (Fig. 8.33). It was G. P. L. Walker (1970, 1973a) who first suggested that magma discharge rate was perhaps the single most important factor governing lava flow morphology and the distances that lavas travelled (Ch. 4), and this appears to be the same for ignimbrites. For most ignimbrites it is not possible to determine discharge rate. However, J. V. Wright (1981) and C. J. N. Wilson and

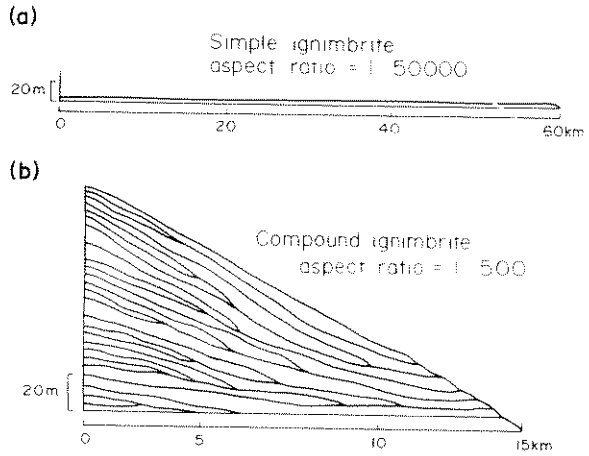

Figure 8.33 Simple and compound ignimbrites. Relationships between thickness, number of flow units and distance travelled are shown schematically for two ignimbrites with similar volumes. (After J. V. Wright 1981.)

Walker (1981) managed to make an estimate for the Rio Caliente and Taupo ignimbrites, respectively, and these are used as the basis for Figure 8.34, together with other data available in the literature.

From the scenario suggested in Figures 8.33 and 34 we can make an assessment of where the Bandelier ignimbrites, and therefore our facies model derived from them, are positioned within this spectrum of ignimbrite types, and also an order of magnitude estimate of their magma discharge rates. Consideration of aspect ratio (1 : 500), number of flow units and proportional volume of

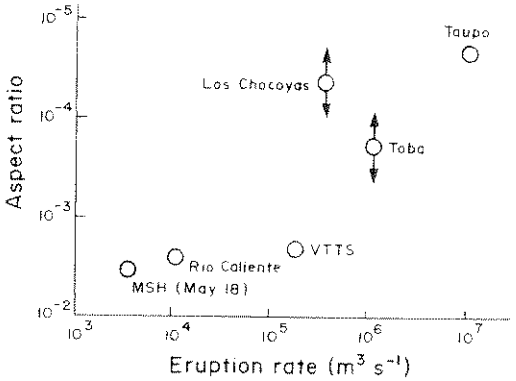

Figure 8.34 Plot of aspect ratio against the average volumetric eruption rate of magma for a number of ignimbrites. Arrows for the Los Chocoyas and Toba ignimbrites indicate uncertainty in measuring aspect ratio.

fine ash lost suggests that both of the Bandelier ignimbrites are towards the lower end of the discharge rate spectrum, and that they have discharge rates of about 10^5 m^3 s^{-1}.

8.8 Palaeocurrent indicators

Flow direction has been determined for a number of ignimbrites by measuring the preferred orientation of elongate crystals and lithic fragments (K. Suzuki & Ui 1982), tree logs (Froggatt *et al.* 1981), welding fabrics (Elston & Smith 1970, Rhodes & Smith 1972, Kamata & Mimura 1983) and magnetic fabrics (Ellwood 1982). K. Suzuki and Ui (1982) have shown that flow orientation was strongly controlled by the pre-existing topography for the Ata pyroclastic flow deposit. Flow lineations oriented radially away from source were only obtained for samples collected from the surface of the ignimbrite sheet. Samples collected from the bottoms of valley-fill deposits had lineations parallel to the axis of the valleys. Samples collected from valley walls tended to be parallel to the slope of the valley. Froggatt *et al.* (1981) also noted that in the Taupo ignimbrite the orientation of tree logs in areas far from the source was parallel to valley axes, even though these could be perpendicular to the general outflow direction.

Wolff and Wright (1981) showed that directional fabrics in welded tuffs are strongly controlled by local palaeoslope. The fact that ignimbrites generally slope away from their source volcano has suggested to some workers that these directional fabrics are likely to reflect flow direction. However, above, we have shown that this line of reasoning is not valid. This short discussion therefore suggests that caution is needed when palaeocurrents of ignimbrites are measured, especially in ancient examples, where they are used to locate source vents. Contouring average maximum lithic clast sizes is the alternative method.

K. Suzuki and Ui (1982) also noted large depositional ramps on the original surface of the Ata pyroclastic flow deposit which provide an independent flow direction indicator. These are shown by the asymmetric distribution of elevation and thickness of deposits in valleys and basins, with deposits ramped up higher on vent-facing slopes. Depositional ramps are also recognised in cross sections through the Ito pyroclastic flow deposit (Fig. 8.3).

8.9 Secondary deposits

Some ignimbrites are obviously interbedded with and overlain by secondary deposits derived from the ignimbrite (e.g. Figs 5.16b & 7.15). These include variously pumiceous mud flows, torrent deposits, lacustrine sediments, reworked wind deposits (Ch. 10) and locally generated phreatic ashes.

Pumiceous mud-flow deposits can closely resemble ignimbrite, and be difficult to distinguish. J. V. Wright (1978) showed that mud-flow deposits interbedded with the Minoan eruption sequence on Santorini could be distinguished from ignimbrite flow units by the absence of a thermal remanent magnetism. Segregation pipes indicating that they had a continuous gas phase, may also be used to identify ignimbrite deposits. However, if mud flows have been generated by water flooding into still-hot ignimbrite, then similar pipes could form but, in these, clasts may be mud-coated and entrapped vesicles may be present in the muddy matrix. Note also that Sheridan *et al.* (1981) have indicated that some pumiceous mud flows could be *primary* products formed at vent during hydrovolcanic phases of ignimbrite-forming eruptions. Torrent deposits that are rich in large lithic blocks may be difficult to distinguish from co-ignimbrite breccias, and pumiceous examples may be hard to differentiate from surge deposits. Angle of repose cross-stratification (Ch. 10), if present, indicates an alluvial origin. Lacustrine deposits will form where river valleys have been blocked by debris. Deposits could include ash turbidites and fines-free assemblages of coarse, very well rounded pumices representing pumice rafts which formed a floating layer on the surface of the lake (Ch. 10). Wind reworking of the top of an ignimbrite could produce stratified and low angle cross-stratified layers which would closely resemble ash-cloud

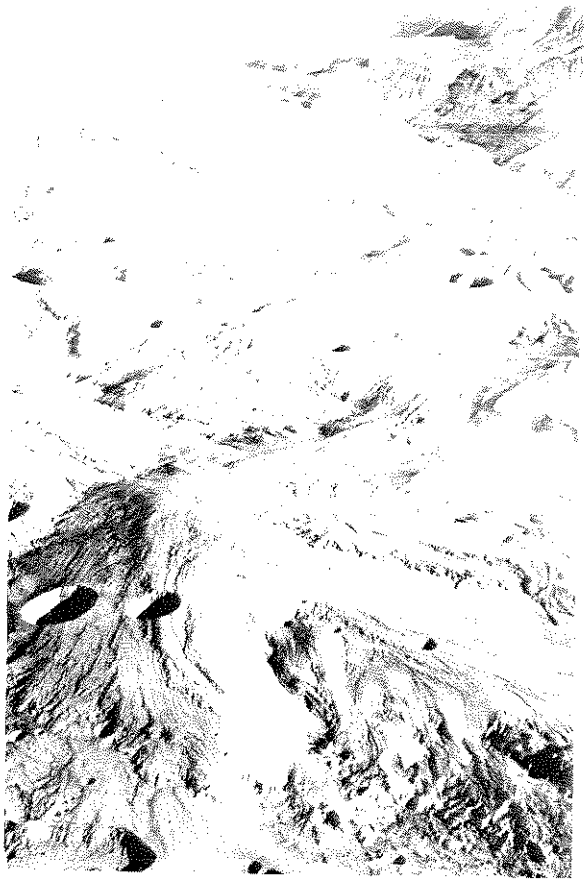

Figure 8.35 Phreatic explosion craters in the 18 May pumice flow deposits on the western part of the Pumice Plain at Mt St Helens (Fig. 8.6). Craters are approximately 5–25 m in diameter. (After Rowley *et al.* 1981.)

surge deposits. However, wavelength and size would not be related to pumice-flow transport direction. On a larger scale, wind erosion can strip large volumes of ignimbrite, adding this to a loess blanket as has happened in New Zealand. Without knowing the regional stratigraphy, such a deposit is probably difficult to distinguish from an air-fall ash deposit at some outcrops (Fig. 10.32b; Section 10.3).

Where large quantities of water gain access to a still-hot ignimbrite, steam explosions can be triggered. These form rootless explosion craters like those observed at Mt St Helens (Fig. 8.35), where local phreatic surge and ash-fall layers were also generated. Similar stratified deposits formed by steam explosions occur above the Taupo ignimbrite (C. J. N. Wilson & Walker 1985) and Crater Lake pumice flow deposit (Bacon 1983).

8.10 Welding and post-depositional processes

Ignimbrites are emplaced at high temperatures and welding, recrystallisation and alteration may occur during the period of cooling. Three main processes can be recognised:

welding
vapour-phase crystallisation
devitrification

8.10.1 WELDING

Welding is the sintering together of hot pumice fragments and glass shards under a compactional load (R. L. Smith 1960a, b; Ross & Smith 1961). The most important controls are:

(a) glass viscosity (dependent on temperature and composition) and
(b) lithostatic load (dependent on the thickness of the deposit).

Lithic content in a deposit will also affect the development of welding (Eichelberger & Koch 1979). Experimental studies indicate that welding begins between about 600 and 750°C for rhyolitic compositions, depending on load pressure and H_2O content of the glass (J. Friedman *et al.* 1963; Bierwirth 1982; Fig. 8.36).

Characteristically, when welding approaches completion, three zones of dense welding, partial welding and non-welding are produced (Fig. 8.37; R. L. Smith 1960b). In the welded zones flattened, often glassy juvenile clasts called fiamme, and glass shards define a planar foliation or eutaxitic texture (Figs 8.38 & 3.23b). In most cases fiamme seem to be flattened pumice clasts, but sometimes they may have originally been unvesiculated juvenile clasts (Gibson & Tazieff 1967). Welding is often associated with distinctive colour changes, which are due to different oxidation states of iron. In densely

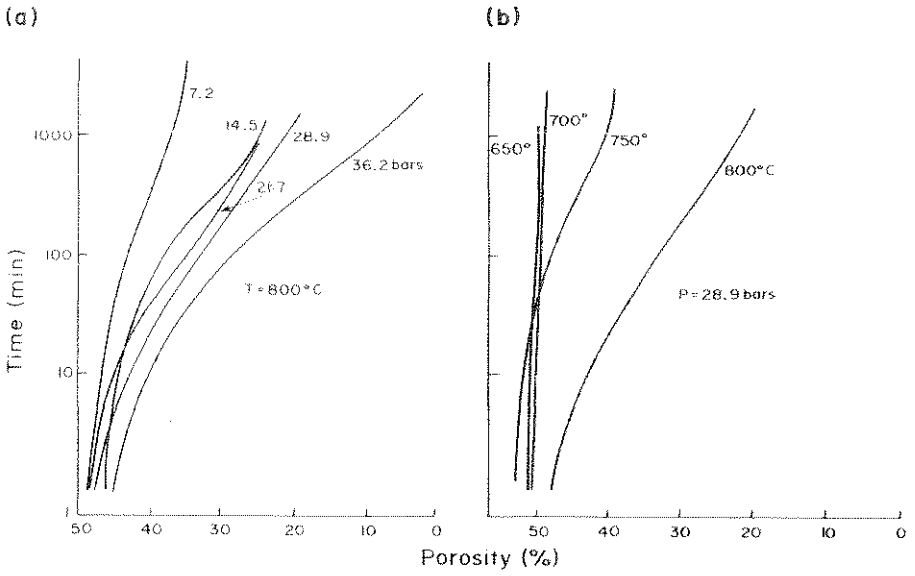

Figure 8.36 Experimentally derived compaction curves for anhydrous rhyolitic ash (<2 mm) from the Upper Bandelier ignimbrite (a) At a constant temperature of 800°C and load pressures of 7.2, 14.5, 21.7, 28.9 and 36.2 bars. (b) At a constant load pressure of 28.9 bars and temperatures of 650, 700, 750 and 800°C. (After Bierwirth 1982.)

welded zones columnar cooling joints are often well developed (Fig. 8.39). Lithophysae may also be present (Fig. 8.37; Ch. 5). A densely welded tuff, which in hand specimen has a glassy appearance, is sometimes called a **vitrophyre**.

Many workers have recorded systematic changes with height in bulk density and porosity in welded ignimbrites (Fig. 8.40). Typically, bulk density is at a maximum, whereas porosity is at minimum in the lower central half of the deposit, and this corresponds to the zone of dense welding. Ragan and Sheridan (1972) showed in the Bishop Tuff that these features are related to the degree of flattening of the pumice clasts, which can be considered a measure of the compactional strain (Fig. 8.41). Strain ratio (see also Figs 6.42 & 45) can be measured in welded tuffs by applying techniques developed by structural geologists to measure tectonic strain (Ramsay 1967, Dunett 1969, Elliot 1970, Lisle 1977, B. Roberts & Siddans 1970, Ragan & Sheridan 1972, Sheridan & Ragan 1976, Sparks & Wright 1979, Wolff & Wright 1981).

R. L. Smith (1960b) classified ignimbrites that showed such simple welding variations as simple cooling units. Riehle (1973) found that these variations could be predicted from theoretical

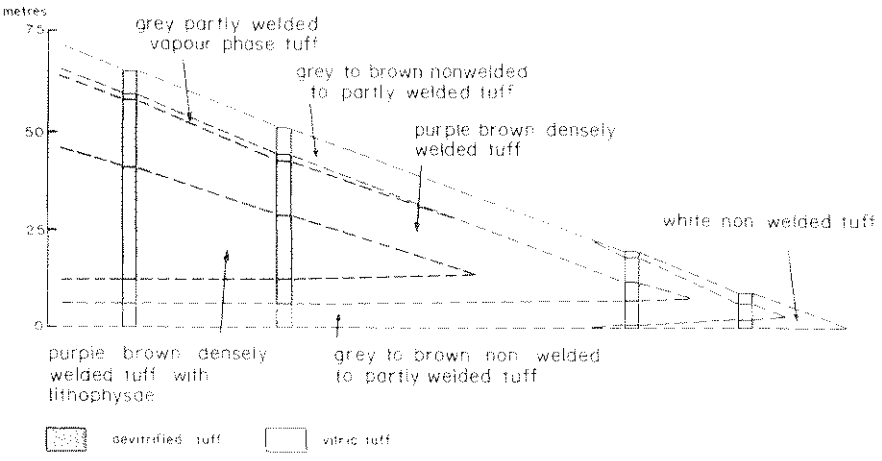

Figure 8.37 Schematic cross section based on four measured sections of the Yucca Mountain Tuff showing welding and devitrification zones in an ignimbrite. (After Lipman & Christiansen 1964.)

6 Experiment-
l compaction
nhydrous rhyolitic
n from the
der ignimbrite.
istant
e of 800°C and
ures of 7.2, 14.5,
and 36.2 bars. (b)
ot load pressure
and
es of 650, 700,
0°C. (After
982.)

e considered a
n (Fig. 8.41).
& 45) can be
ing techniques
s to measure
tt 1969, Elliot
Siddans 1970,
& Ragan 1976,
ight 1981).
gnimbrites that
ions as simple
nd that these
m theoretical

Schematic
n based on four
ections of the
ain Tuff
ding and
n zones in an
After Lipman &
1964.)

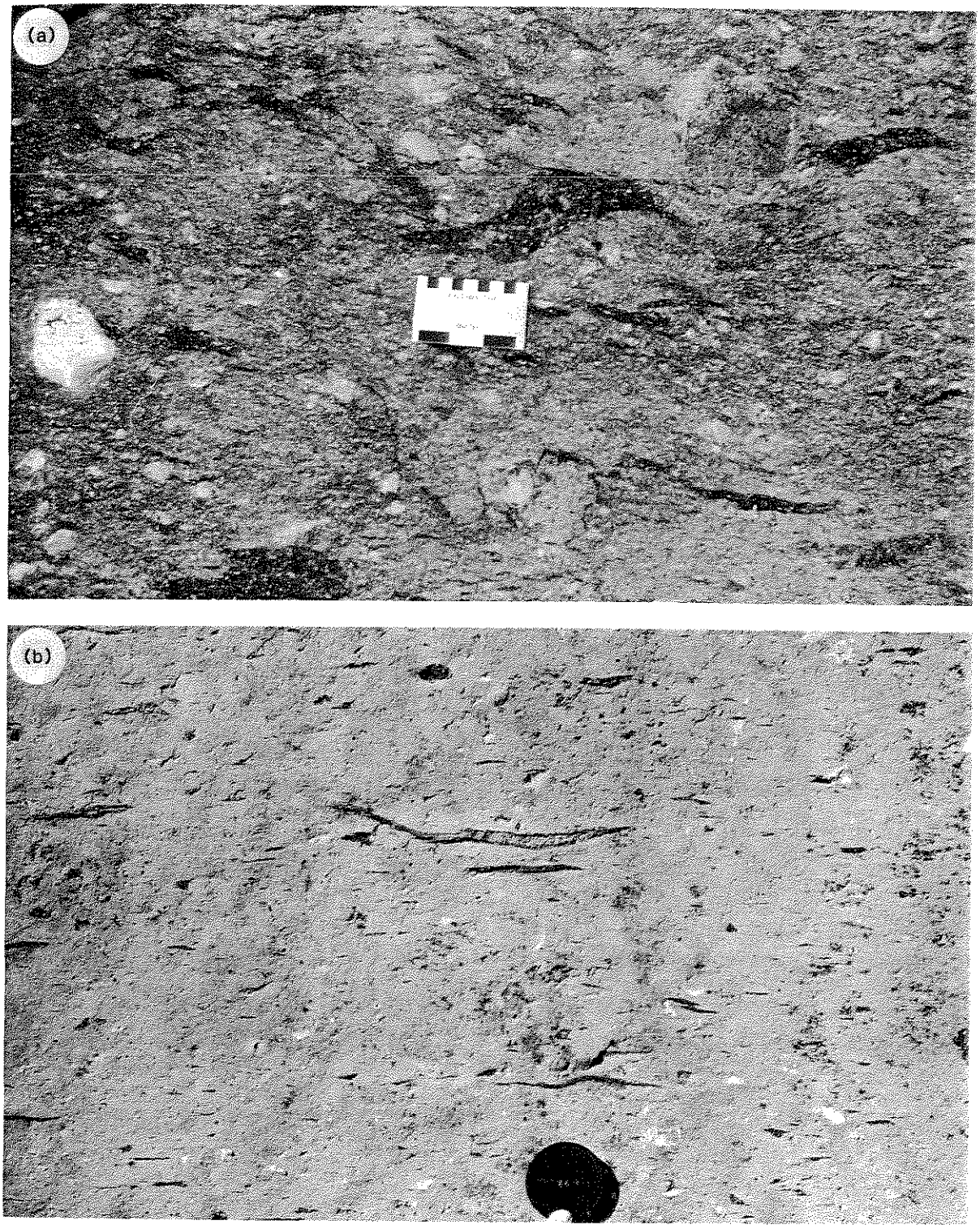

Figure 8.38 Welded ignimbrites with eutaxitic textures defined by fiamme. (a) Ignimbrite erupted from Platoro caldera (part of Treasure Mountain Tuff), San Juan volcanic field, Colorado. (b) Very densely welded ignimbrite near La Piedad, Central Mexico.

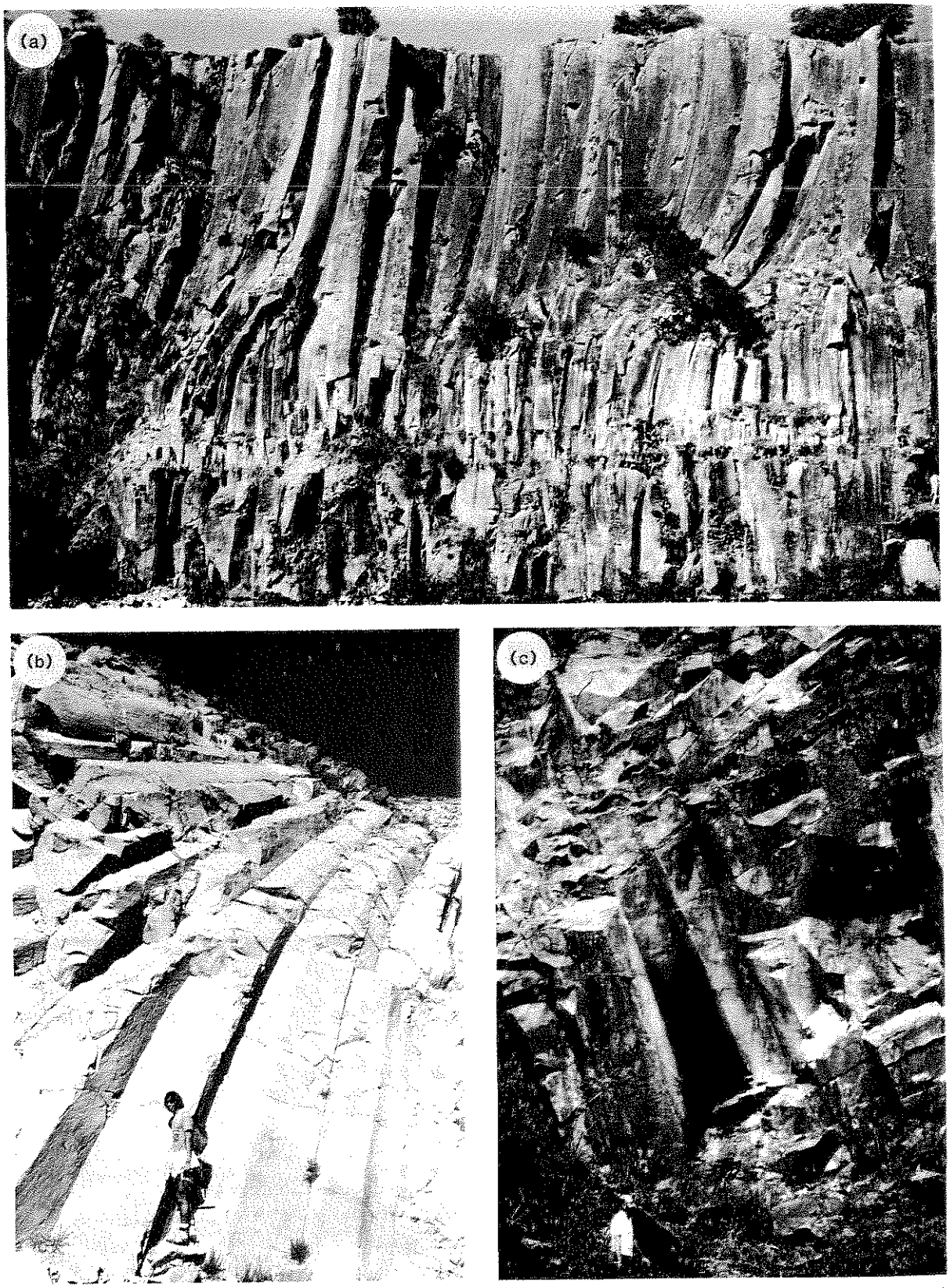

Figure 8.39 Columnar jointing in welded ignimbrites. (a) Amealco ignimbrite (Quaternary), near San Juan del Rio, Central Mexico. (b) Bishop Tuff, California. (c) Rubicon Rhyolite (Devonian), Central Victoria, Australia.

el Rio, Central

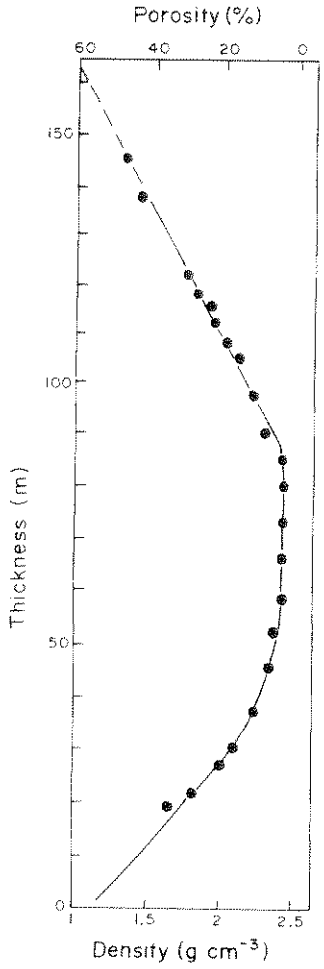

Figure 8.40 Density–porosity profile for the Bishop Tuff. (After Ragan & Sheridan 1972.)

analysis of the cooling of a sheet emplaced with uniform temperature. However, some ignimbrites have several zones of dense welding and partial welding. Such ignimbrites are classified by Smith as **compound cooling units** (Fig. 8.42). These suggest that the upper parts of earlier flow units of the ignimbrite must have been partially or wholly cooled before the emplacement of later flow units. Some care must be taken when describing compound cooling units, as they may even consist of a number of ignimbrites separated by long intervals between eruptions.

Most welded rocks only show compactional flattening of fiamme and glass shards (Fig. 8.41). However, in some welded tuffs fiamme are seen to be stretched, and in sections parallel to the plane of foliation of fiamme they show a well defined lineation (Fig. 8.43). This indicates secondary mass flowage of the tuff during welding, and is termed **rheomorphism**. Flow folds are sometimes also well developed. Schmincke and Swanson (1967) and other workers (e.g. Chapin & Lowell 1979) have suggested that stretching and welding of fiamme may be a primary flow feature during the final stages of pyroclastic flow. Wolff and Wright (1981) argued that it must be a secondary process involving first compactional deformation and then subsequent flow on a slope. Many (but not all) examples of rheomorphic welded tuffs are peralkaline rhyolites having unusually low glass viscosities compared with calc-alkaline rhyolites.

Ignimbrites which show well developed zones of dense welding, and in which the proportion of welding is high, can be termed **high-grade ignimbrites**, in contrast to **low-grade ignimbrites**, which are totally non-welded or of which only a small proportion is welded. The temperature of emplacement of ignimbrites is therefore very variable. R. L. Smith (1960a) considered that processes within the eruptive column must be responsible, and Sparks *et al.* (1978) explained this by the eruption column collapse model. Eruptions with low gas content and low gas velocity will lead to low collapse heights and little heat loss during collapse.

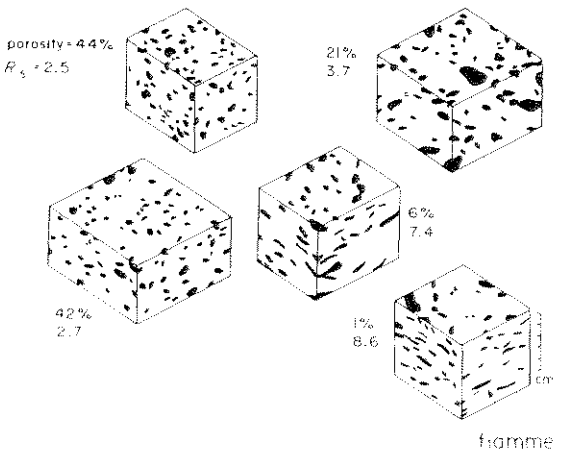

Figure 8.41 Cut blocks of Bishop Tuff, showing increase in flattening of pumice clasts with decreasing porosity. Values of strain ratio (R_s) show the increasing compactional strain. Note block (c) is cut slightly oblique to the foliation. (After Ragan & Sheridan 1972.)

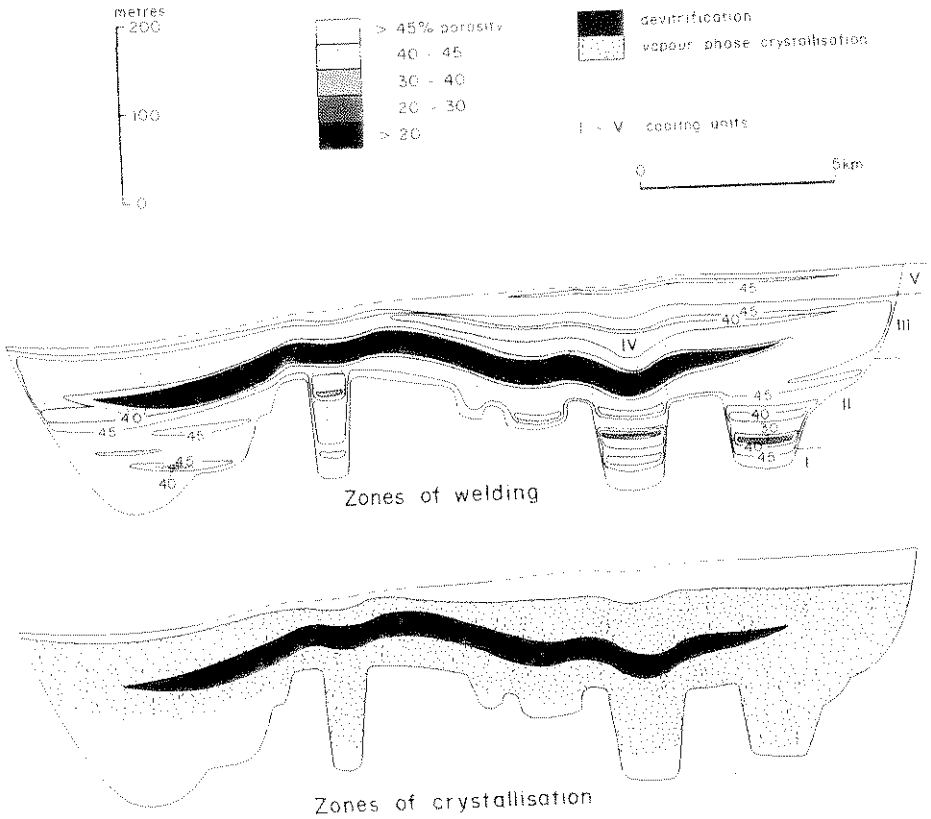

Figure 8.42 Cross section through part of the Upper Bandelier Tuff, showing welding and crystallisation zones. The ignimbrite is a compound cooling unit, and shows an upward increase in the degree of welding in cooling units I–III. Recognisable flow units are much thinner in units IV and V, and nearer the source they pass into densely welded tuff, continuing the trend towards higher temperature of emplacement of successive pumice flows that is more clearly shown by units I–III. Note, the topography that the ignimbrite fills in is cut into older ignimbrites and basement, including Precambrian (cross section is approximately normal to movement direction of the pumice flows). (After R. L. Smith & Bailey 1966.)

which will favour formation of a densely welded ignimbrite. This condition will also lead to less-expanded flows which should lose only minor amounts of vitric ash, as seems to be the case for many densely welded intracaldera ignimbrites (Section 8.4; Ch. 11). Flows formed from high collapse heights will be emplaced at relatively lower temperatures, and may form non-welded deposits. Some large ignimbrites show an upward increase in welding due to the emplacement of flow units of successively higher temperature. The Upper Bandelier ignimbrite shows such a sequence, with flow unit temperatures changing from the order of 550–800°C (R. L. Smith & Bailey 1966; Fig. 8.44). Widening of the vent and a decrease in gas content during eruption and column collapse could both explain increasing emplacement temperature.

The time taken to produce welding has been estimated theoretically by Riehle (1973) and Kono and Osima (1971). However, their methods are based on the assumption that viscous strain occurs, but this is incorrect for porous volcanic ash because it does not allow for the effects of pore space (porosity) and packing geometry. Bierwirth (1982) considered the effects of porosity as shown by models of sintering and hot pressing processes used in the ceramic and metallurgical industries. The strain rate for porous materials is given by

$$\dot{\epsilon} = Kf(\varrho)P^n e^{-Q/RT} \qquad (8.1)$$

where, T is temperature, P is load pressure, Q is activation energy, n is a stress factor, $f(\varrho)$ is a density function, R is the universal gas constant and K is the strain rate constant. Using the results of his Bandelier Tuff experiments (Fig. 8.36), values of Q, n and K were determined and a nearest-fit equation assigned to $f(\varrho)$. After converting strain to density, Equation 8.1 was integrated giving an equation defining compaction rates of anhydrous ash from the Bandelier Tuff:

e 8.42 Cross
r through part of
pper Bandelier Tuff,
ing welding and
illisation zones. The
bnite is a compound
g unit, and shows
vard increase in
egree of welding in
g units I–III
onsable flow units
uch thinner in units
d V, and nearer the
e they pass into
ely welded tuff, con-
g the trend towards
r temperature of
acement of succes-
pumice flows that is
clearly shown by
I–III. Note, the
graphy that the
bnite fills in is cut
older ignimbrites
basement, including
ambrian (cross
on is approximately
al to movement
tion of the pumice
). (After R. L. Smith
dley 1966.)

ous strain occurs,
canic ash because
is of pore space
Bierwirth (1982)
ity as shown by
ng processes used
l industries. The
given by

$$/RT \qquad (8.1)$$

ad pressure, Q is
factor, $f(\varrho)$ is a
rsal gas constant
Using the results
nts (Fig. 8.36),
termined and a
). After convert-
.) was integrated
paction rates of
r Tuff:

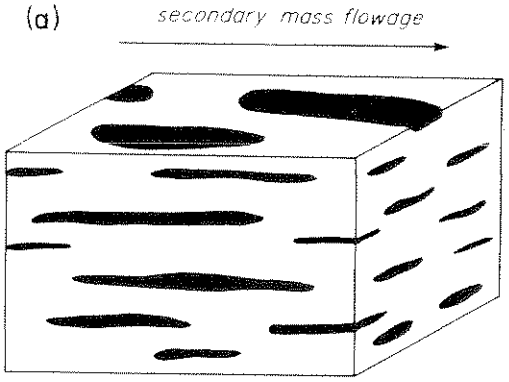

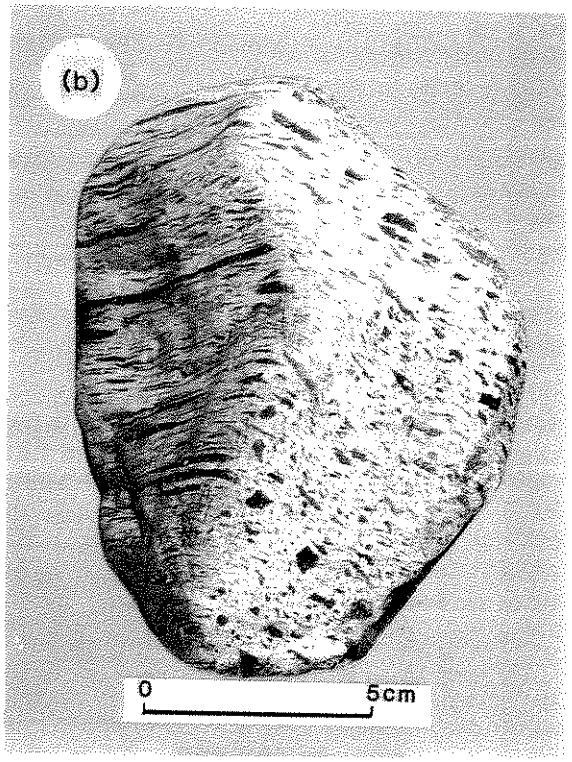

Figure 8.43 Lineation produced by stretching fiamme during rheomorphism.

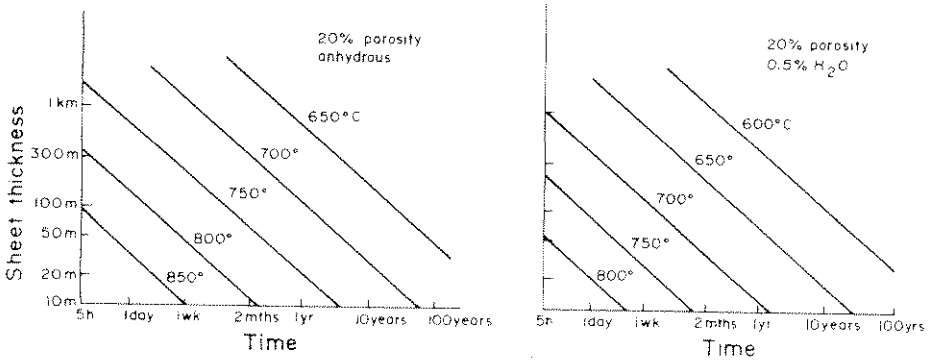

Figure 8.44 Time required to produce dense welding of rhyolitic ash (a) anhydrous and (b) with 0.5 wt% water for various ignimbrite thicknesses and emplacement temperatures. Calculated from Equation 8.2 based on experimental studies of the Upper Bandelier ignimbrite. The model is least reliable for thin flows and long times, due to the effects of cooling. Sheet thickness was calculated for porous ash (1 bar = 7 m). (After Bierwirth 1982.)

$$19.7\varrho^{11} + 0.04\varrho^{-1} - 0.092 = (6.3 \times 10^{15} P^{1.7} e^{-5.6} \times 10^{4/T})t \qquad (8.2)$$

where ϱ is fractional density, t is time in seconds, P is in bars and T in K.

Values are reliable for fractional densities less than 0.9 (<2.4 g cm^{-3}, >10% porosity). Equation 8.2 produces values which correlate well with experimental results, and enables predictions to be made beyond the time range of experiments. For an ignimbrite 100 m thick and emplaced at 850°C, dense welding (<20% porosity) would occur within

one week (Fig. 8.44a). For even a 1 km thick intracaldera ignimbrite at 650°C, dense welding would only be achieved after one year, assuming that crystallisation of the groundmass did not prevent compaction. Welding temperatures will be lowered by the effect of water content in the glass, and the times shown in Figure 8.44a can be regarded as maximum values. Bierwirth indicated that 0.5 wt% water will lower welding temperatures by approximately 60°C compared with anhydrous conditions (Fig. 8.44b).

8.10.2 VAPOUR-PHASE CRYSTALLISATION

Vapour-phase crystallisation results from the percolation of hot gases through ignimbrites during cooling. The most important gas sources are probably diffusion from juvenile vitric particles and heated ground water.

The main products of vapour phase crystallisation are tridymite, cristobalite and alkali feldspar, which occur as drusy infills of matrix and pumice cavities, so forming a cement and reducing the pore space. Vapour-phase crystallisation can produce a coherent rock. The term sillar (a Peruvian word first applied by C. N. Fenner 1948) is often used for such rocks, but the term has also been applied to incipiently welded tuffs in which ash grains are barely sintered at point contacts and show no other deformation of juvenile clasts (Fig. 8.7). Vapour-phase crystallisation can occur in separate zones in compactionally welded ignimbrites, and is commonly found towards the top of a sheet (Figs 8.37, 42 & 45). Sheridan (1970) described fumarolic mounds and ridges of sillar above the Bishop Tuff (Figs 8.45 & 46a). Similar palaeofumarolic features and peculiar '*steam pipes*' occur in the Rio Caliente ignimbrite, which are thought to have formed where it was deposited in a shallow lake or on marshy ground (Figs 8.46b, c & 47). Fumarolic pipes have also been found in the Bandelier ignimbrites (Fig. 8.46d).

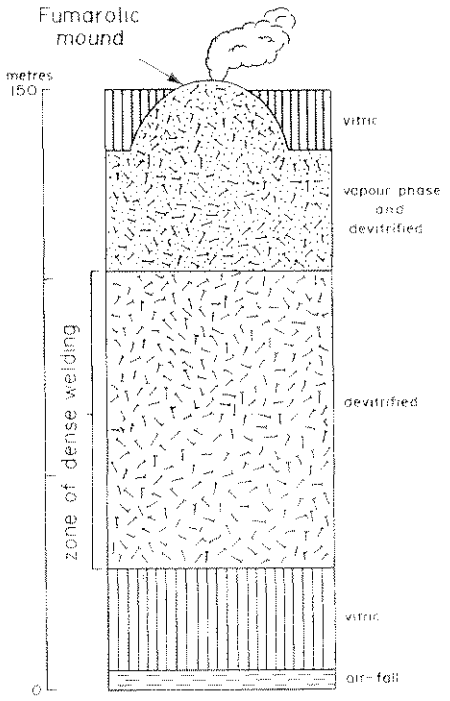

Figure 8.45 Zones of vapour-phase crystallisation and devitrification in the Bishop Tuff. Fumarole mounds project from top of vapour-phase zone through non-welded ash. (After Sheridan 1970.)

8.10.3 DEVITRIFICATION

Devitrification involves the sub-solidus crystallisation of metastable glass (Ross & Smith 1961, Lofgren 1970). The main products are cristobalite and alkali feldspar. Devitrification tends to be more prevalent in densely welded tuffs, and particularly in thick intracaldera ignimbrites because of the protracted cooling (Figs 8.37, 42 & 45). Nevertheless, more-porous ignimbrites may also be devitrified. (Note that devitrification is also common in coherent glassy lavas and shallow intrusives.) Devitrification is discussed further in Chapter 14 (Section 14.3.2).

8.11 Chemical analyses?

Post-depositional chemical alteration is a common feature even of *modern* ignimbrites. There are several processes which can produce alteration. One is leaching by ground water, and studies show that metastable glass is easily leached and Na, K and Si are often removed (e.g. Noble 1967, Scott

eldspar,
pumice
the pore
oduce a
in word
en used
applied
ains are
no other
Vapour-
zones in
is com-
igs 8.37,
umarolic
iop Tuff
features
Caliente
formed
se or on
umarolic
Bandelier

crystallis-
ith 1961,
ristobalite
o be more
rticularly
se of the
Neverthe-
ne devitri-
ommon in
ntrusives.)
hapter 14

a common
There are
alteration.
udies show
and Na, K
1967, Scott

Figure 8.46 (a) Fumarole mounds on the surface of the Bishop Tuff. (b) and (c) Small '*steam pipes*' in the Rio Caliente ignimbrite. Vapour phase minerals are predominantly clinoptilolite and heulandite which suggests low temperature fumarolic activity (compared with tridymite, cristobalite and alkali feldspar, which are the usual vapour phase minerals found, e.g. in the Bishop Tuff). This is as might be expected if the ignimbrite were locally deposited in a shallow lake or on marshy ground and vaporised ground water was important. (d) Fumarole pipes in the Upper Bandelier Tuff.

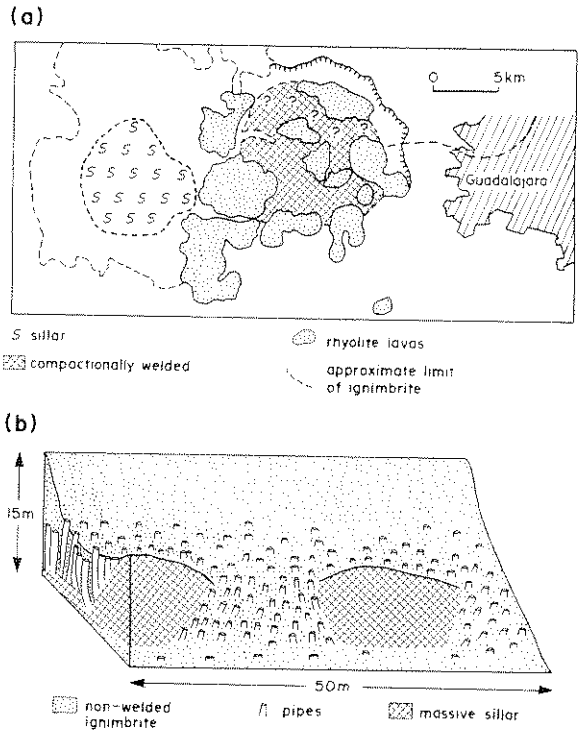

Figure 8.47 (a) Map showing distribution of sillar and palaeofumarolic area in the Rio Caliente ignimbrite, New Mexico. (b) Field sketch showing relations in the area shown in Figure 8.47a. Pipes are radially distributed about massive zones of sillar, which seemed to have been the sites of most intense vapour-phase activity.

1971). Vapour phase and fumarolic activity and hot springs related to the regional geothermal system (Fig. 13.48) is the second important source of alteration (see the previous section).

Both Ui (1971) and G. P. L. Walker (1972) warn against the acceptance of whole rock analyses of ignimbrites as guides to the composition of the parent magma. Such analyses are subject to considerable error, because of the presence of xenoliths in the lithic component (Ui 1971). Perhaps more important, though, is the concentration of crystals that is found in ignimbrites due to the selective loss of fine vitric ash during eruption and emplacement. The composition of the ignimbrite will be enriched in those elements occurring in higher proportions in the crystals, and will be depleted in those occurring in higher proportions in the glass.

The above questions the value of chemical analyses of ignimbrite (especially whole rock analyses of ancient welded ignimbrites), and indicates the care needed in sampling.

8.12 The great Taupo AD 186 eruption

The studies by G. P. L. Walker, C. J. N. Wilson and co-workers on the products of this ignimbrite-forming eruption have greatly stimulated volcanology, yielding new insights into explosive volcanism and extending the range and scale of known volcanic phenomena. A brief eruption narrative is, therefore, a fitting finale to this chapter. The eruption produced a great variety of pyroclastic products, including the most powerful plinian and most violent ignimbrite-forming events yet documented (Chs 6 & 7; Section 8.7). It is the youth and excellent preservation of the deposits that enabled the eruption sequence to be examined in such detail.

The products of the Taupo eruption (Figs 8.48 & 49) are dispersed over a large part of the North Island of New Zealand. They consist of: an initial plinian pumice-fall deposit, the Hatepe pumice; two phreatoplinian ashes, the Hatepe ash and the Rotongaio ash, which are separated from each other by an erosional break; an ultraplinian pumice-fall deposit, the Taupo pumice; and, finally, the

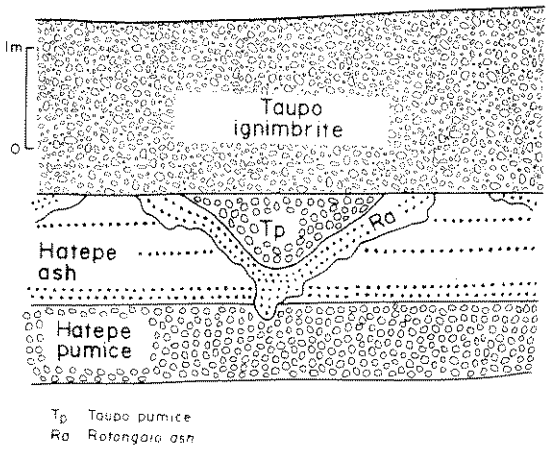

Figure 8.48 Stratigraphy of the products of the Taupo AD 186 eruption, New Zealand. (After G. P. L. Walker *et al.* 1981a.)

hole rock analy-
and indicates

6 eruption

J. N. Wilson
this ignimbrite-
mulated volca-
xplosive volcan-
scale of known
ion narrative is,
chapter. The
of pyroclastic
rful plinian and
vents yet docu-
s the youth and
its that enabled
mined in such

tion (Figs 8.48
rt of the North
ist of: an initial
latepe pumice;
pe ash and the
from each other
an pumice-fall
l. finally, the

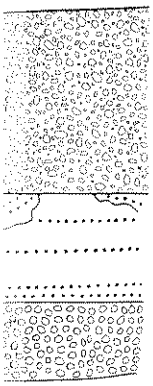

of the Taupo AD
L. Walker *et al.*

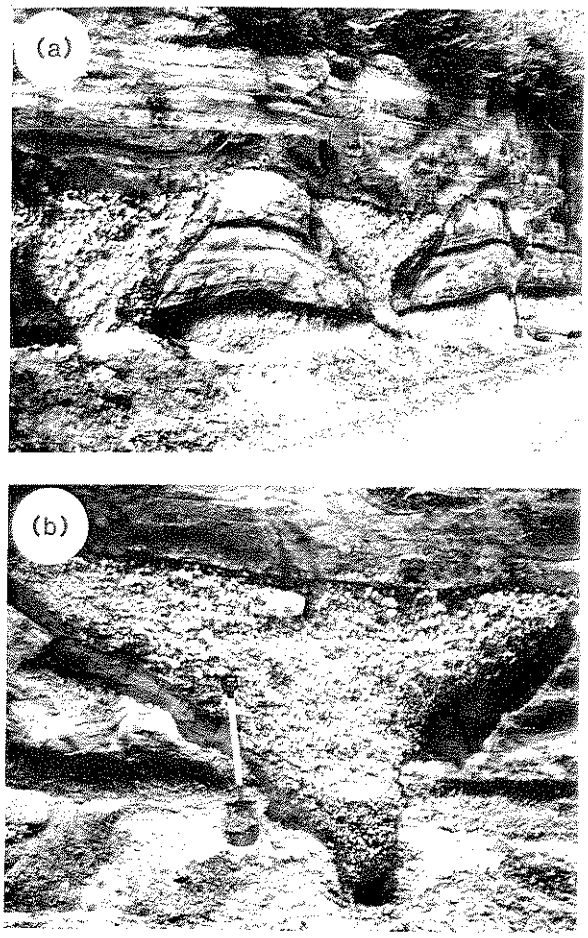

Figure 8.49 The Taupo eruption sequence as explained in Figure 8.48, showing prominent infilled erosion gullies between the Hatepe and Rotongaio ashes, and strongly discordant erosion surface between the Taupo ignimbrite and Taupo pumice. This location is 20 km ESE of the vent. (Photographs by C. J. N. Wilson.)

climactic Taupo ignimbrite. The total erupted volume was about 100 km^3 (dense rock equivalent), of which 24 km^3 is found in the Taupo ultraplinian pumice-fall deposit, 30 km^3 in the Taupo ignimbrite and another 20 km^3 in a co-ignimbrite ash fall. In this section we briefly consider some of the exceptional features of this sequence.

From various lines of evidence, the vent position is inferred to be at or near the Horomatangi Reefs in Lake Taupo. Horomatangi Reefs may be lava domes or the remnants of a pyroclastic cone. The sequence of phases can be interpreted in terms tumescence of the vent area or loss of lake water, exposing a dry-land vent, and subsequent de mescence submerging the vent during the erupti (Fig. 8.50).

We will now consider the principal phases of t Taupo eruption:

early air-fall phases
Taupo ultraplinian fall deposit
Taupo ignimbrite

8.12.1 EARLY AIR-FALL PHASES

The Hatepe pumice is a coarse, relatively hom geneous and well sorted layer which shows man bedding. Its dispersal (Fig. 8.51a) and grainsi characteristics are typically plinian.

The two phreatoplinian layers (Figs 8.51b & are fine-grained, stratified, relatively poorly sort ash deposits (G. P. L. Walker 1981a). Both sho very little change in grainsize and sorting wi distance from source. They both show many sig of being deposited as 'wet' ash. For example, t Hatepe ash locally shows a type of microbeddi attributed to the splashing of falling water; bo deposits contain vesicles formed when air w trapped by ash falling as sticky mud; the Rotonga ash, where thick, often slid as small mud flows in the gullies cut into the Hatepe ash; and sof sediment deformation structures are found (Fi 8.52). However, both lack accretionary lapilli, b very wet accretionary lapilli similar to mud-ra could have easily splashed on impact. The poo sorting of the deposits is attributed to wate scavenging of the ash cloud. Although they on show limited fractionation with distance, bot layers show a regular exponential thinning fro source (Figs 8.51b & c), indicating that th scavenging water must have been derived from th source, Lake Taupo. The water was therefore a integral part of the eruption column and ash clouc and G. P. L. Walker (1981a) envisaged a full water-charged column erupting out of Lake Taupo with both ashes actually falling as mud.

The deep-gullied erosion surface separating th two ash layers is significant, and there is a similar

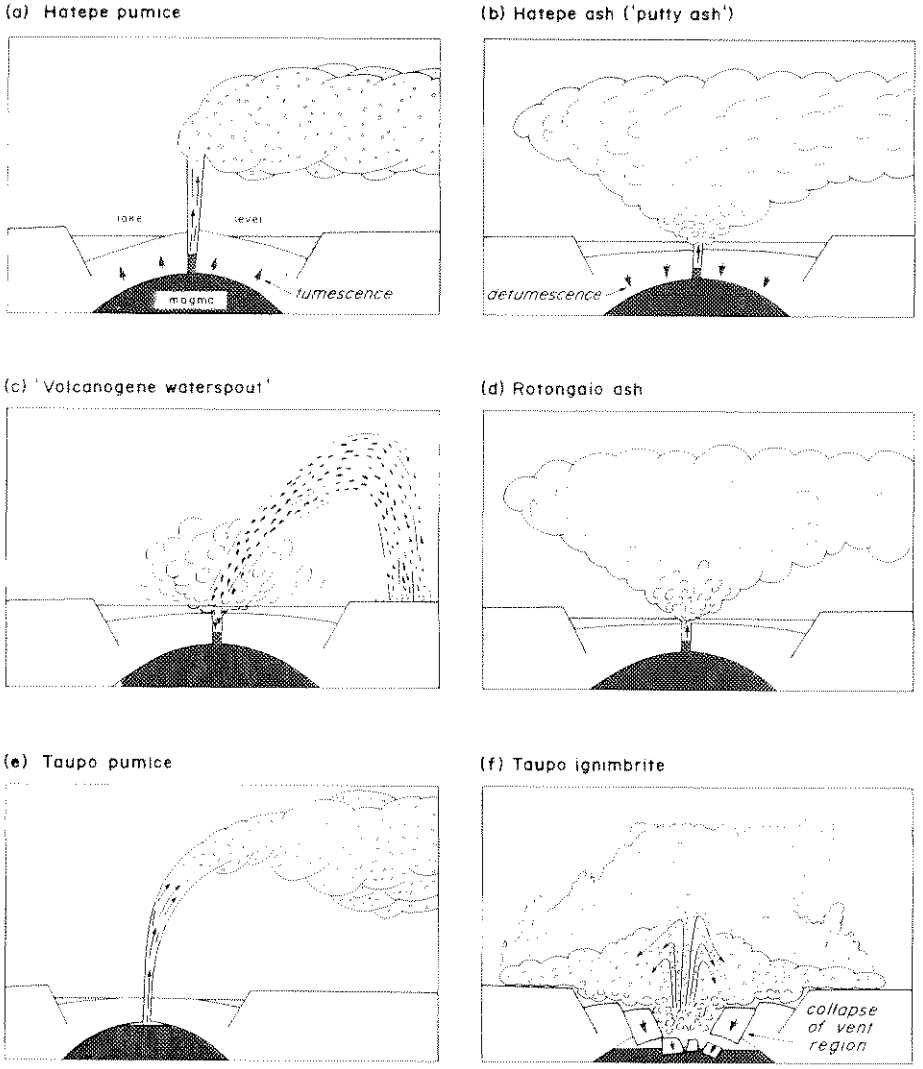

Figure 8.50 Pictorial representation of the different phases of the Taupo eruption.

but less prominent, erosion surface within the Hatepe ash. Features of the gullies indicate very rapid erosion in two brief episodes during the eruption. The depth of gullying, and therefore the amount of erosion, decreases systematically away from Lake Taupo (Fig. 8.53). This strongly suggests that the gully erosion was somehow related to the eruption column, and Walker believes that this was when a large part of the lake was erupted as a giant '*volcanogene waterspout*' (Fig. 8.50c).

8.12.2 TAUPO ULTRAPLINIAN FALL DEPOSIT

The Taupo pumice is extensively described by G. P. L. Walker (1980), who used this deposit to define the term '*ultraplinian*', reflecting its extremely wide dispersal (Fig. 8.54; Ch. 6). It is a coarse pumice fall deposit (Fig. 8.49), which is internally stratified, especially near vent, shows mantle bedding and otherwise resembles a normal plinian deposit on a local scale. Although the maximum lithic and pumice isopleths demonstrate that the

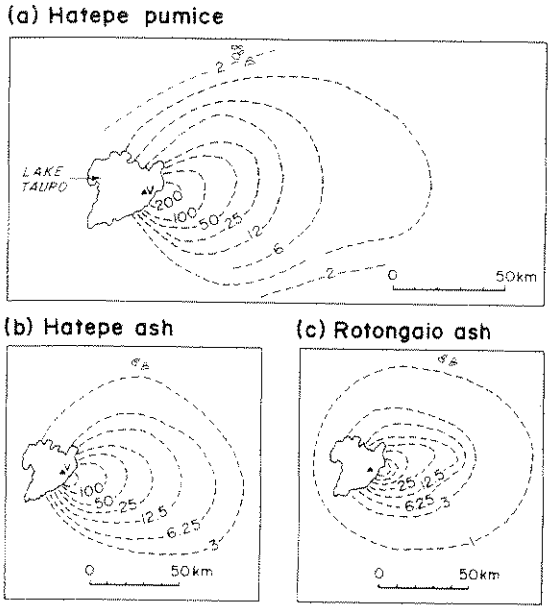

Figure 8.51 Isopach maps illustrating the distribution of the early air-fall phases. (After G. P. L. Walker 1981a & c.)

vent lay within the present Lake Taupo, the isopachs of the deposit close about a point about 20 km east of the lake, a fact which led earlier workers to place a vent on-shore. However, this secondary thickening away from the vent can be explained by the combination of a very high eruption column, partly attributable to a very high eruption rate (estimated at 10^6 m^3 s^{-1} of magma), and a strong westerly wind shifting the eruption column sideways (Fig. 8.50e). Also, at many of the near-source outcrops the Taupo pumice has obviously been eroded by the Taupo ignimbrite which followed, and therefore thickness measurements are anomalously thin.

The maximum measured thickness is only 1.8 m, which reflects the great dispersal of the deposit although, again, even where it is thickest there is a marked erosional discordance between it and the ignimbrite. Despite its *unimpressive* thickness (cf. other plinian deposits, Ch. 6), calculations by G. P. L. Walker (1980) from the concentration of free crystals in the deposit show that the total volume erupted was 24 km^3 (6 km^3 dense rock equivalent (DRE)), which is as big as some of the

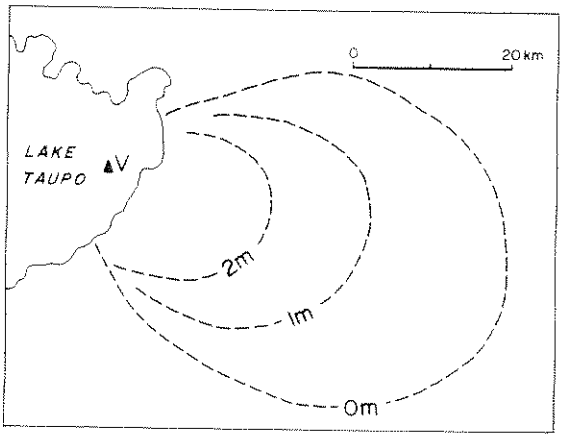

Figure 8.53 Map showing approximate extent of gully erosion in the interval between the eruption of the Hatepe and Rotongaio ashes with isopleths of gully depth. (After G. P. L. Walker 1981a.)

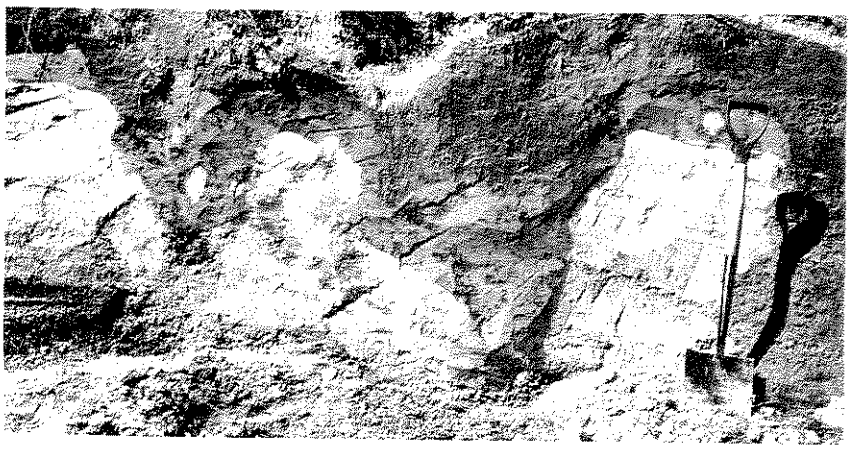

Figure 8.52 Soft-sediment deformation structures between the Hatepe (pale) and Rotongaio (dark) ashes. The contact separating the two is partly erosive (Fig. 8.49). (Photograph by C. J. N. Wilson.)

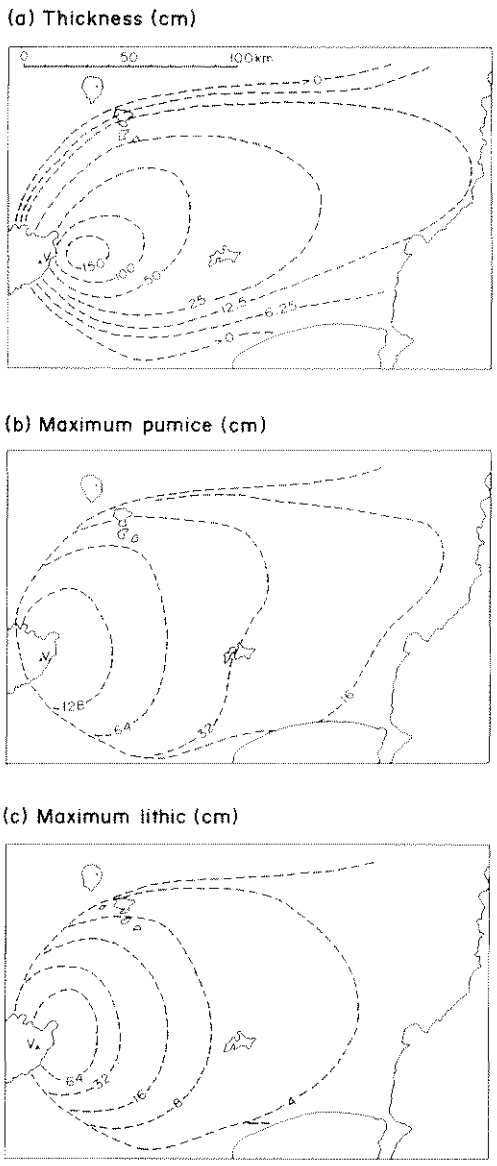

Figure 8.54 Isopach and maximum-size isopleth maps (average diameter of the largest clasts) for the Taupo pumice. (After G. P. L. Walker 1980.)

larger plinian deposits known (Table 6.2). Of this volume only about 20% fell on land, and 80% (mainly finer vitric ash) fell out to sea more than 220 km from source. Independent methods indicate that the height of the eruption column must have been in excess of 50 km, and that this phase lasted 6–17 h.

8.12.3 TAUPO IGNIMBRITE

We have already discussed at length many of the features of this spectacular ignimbrite (Ch. 7; Section 8.7). The abrupt switch from fall- to flow-forming activity is thought to have been caused by a drastic increase in discharge rate (Fig. 8.34), and cannot simply have been due to the collapse of the very high ultraplinian column. C. J. N. Wilson and Walker (1985) suggest that the high eruption rate during the ultraplinian phase drained the upper part of the magma chamber, leaving its roof unsupported. This eventually led to major collapse of the vent region (Fig. 8.50f). This greatly widened the vent, and the ignimbrite-producing flow was then formed by instantaneous column collapse, the discharge rate being suddenly much greater than that which would allow for the maintenance of a stable convective column (Fig. 8.11). The lithic content of the pre-ignimbrite air-fall deposits (1 km^3) implies that vent widening by erosion was important and would eventually have led to column collapse if the eruption had followed a normal course of events. Indeed, occasional partial collapses of the ultraplinian column did occur, generating a number of early ignimbrite flow units found interbedded with the Taupo pumice near the source. A sudden increase in the volume (2 km^3) and sizes of lithics in the Taupo ignimbrite support the idea that there was a drastic change in eruption conditions.

Field data suggest that the parent flow of the Taupo ignimbrite erupted over only 400 s in batches of material which gradually coalesced so that from about 40 km outwards the flow was a single wave of material (C. J. N. Wilson & Walker 1981). During most of its passage, the flow consisted of a head (strongly fluidised by ingested air) which generated layer 1 deposits, and a body plus tail which generated layer 2 deposits (Ch. 7). The flow moved at very high velocities over a locally mountainous terrain at speeds probably exceeding 250–300 m s^{-1} near the vent, and which remained high (locally >100 m s^{-1}) to the outer limits of the flow. The flow-head was highly erosive and locally, almost unbelievably, scalped and overturned the floor over which it rode (Fig. 8.55). A variety of

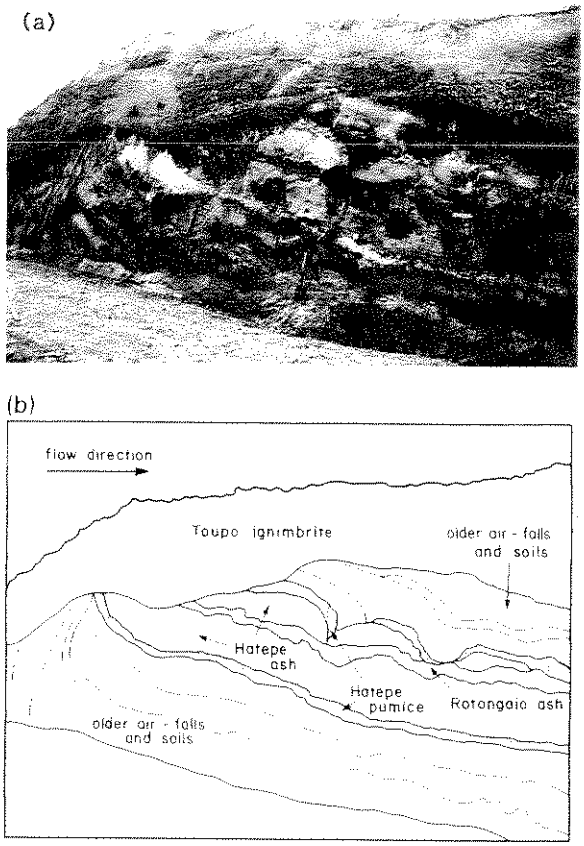

Figure 8.55 The Taupo ignimbrite at this location scalped and overturned air-fall layers of the preceding phases in the eruption and older air-fall deposits and soils. This outcrop is approximately 15 km east of the vent, the Taupo pumice is absent because it was presumably stripped off before the erosive overturning event occurred

processes acting in response to fluidisation or flow kinetics operated within the flow to produce the great variety of facies.

8.12.4 OVERVIEW

The total thickness of air-fall deposits amounts to over 5 m near the vent, nearly all of the material having been blown to the east of the vent by strong south-west to westerly winds (Figs 8.51 & 54). Air-fall deposits more than 10 cm thick were deposited over an area of 30 000 km^2, while an area of about 20 000 km^2 was devastated by the Taupo ignimbrite flow. In addition, mud flows and floods reached far beyond the limits affected by primary eruption products. The total duration of the eruption could have been as short as a few days or as long as months, depending on the length of the time gap between the Hatepe and Rotongaio phreatoplinian phases. If the Taupo eruption were repeated, there can be no doubt how catastrophic its effects would be.

8.13 Further reading

R. L. Smith's classic papers published in the early-1960s (R. L. Smith 1960a, b, Ross & Smith 1961) are still essential reading, having been, for the past two decades, the foundation for the advances in our understanding of ignimbrites. The Geological Society of America has honoured this pioneering work with publication of the Special Paper entitled 'Ash-flow tuffs', edited by Chapin and Elston (1979). This contains some of the more up-to-date information and reviews, including one by Smith himself (R. L. Smith 1979) which looks in some detail at physicochemical aspects of ignimbrite magma chambers. G. P. L. Walker (1983) reviewed ignimbrite types and problems, and in this very useful article 'takes stock of what is known, and also what needs to be known before ignimbrites are well understood'. In addition Walker (1985) has reviewed the origins of ignimbrite-associated breccias. Although much of the Taupo AD 186 story is scattered in a large number of papers, C. J. N. Wilson and Walker (1985) have pieced together an eruption narrative, and C. J. N. Wilson (1985) presents his complete story for the Taupo ignimbrite in an outstanding publication. One other, slightly older, paper worthy of special note is Yokayama (1974), on the Ito pyroclastic flow deposit (Fig. 8.3). An important volume on caldera formation and caldera geology is the special issue of *Journal of Geophysical Research* (1984, volume 89 B10), edited by Lipman, Self and Heiken. The papers by Lipman (1984) and G. P. L. Walker (1984a) in this volume provide interesting contrasts, Lipman high-lighting the complexities of the 'standard' caldera collapse model, including the

changing nature and position of the vent system, whereas Walker puts the 'standard' caldera model into perspective by identifying significant deviations from the standard model in many volcanoes. Fisher and Schmincke (1984) have also given a comprehensive summary of the characteristics of pyroclastic flow deposits.